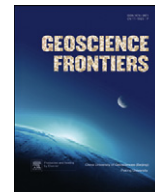


Contents lists available at [SciVerse ScienceDirect](http://www.elsevier.com/locate/gsf)

China University of Geosciences (Beijing)

Geoscience Frontiers

journal homepage: www.elsevier.com/locate/gsf

Research paper

Geochemical constraints on komatiite volcanism from Sargur Group Nagamangala greenstone belt, western Dharwar craton, southern India: Implications for Mesoarchean mantle evolution and continental growth

Tushipokla, M. Jayananda*

Department of Geology, Centre of Advanced Studies, University of Delhi, Delhi 110007, India

ARTICLE INFO

Article history:

Received 2 May 2012

Received in revised form

6 November 2012

Accepted 8 November 2012

Available online 2 December 2012

Keywords:

Komatiites

Dharwar craton

Geochemistry

Greenstone volcanism

Mantle evolution

ABSTRACT

We present field, petrographic, major and trace element data for komatiites and komatiite basalts from Sargur Group Nagamangala greenstone belt, western Dharwar craton. Field evidences such as crude pillow structure indicate their eruption in a marine environment whilst spinifex texture reveals their komatiite nature. Petrographic data suggest that the primary mineralogy has been completely altered during post-magmatic processes associated with metamorphism corresponding to greenschist to lower amphibolite facies conditions. The studied komatiites contain serpentine, talc, tremolite, actinolite and chlorite whilst tremolite, actinolite with minor plagioclase in komatiitic basalts. Based on the published Sm-Nd whole rock isochron ages of adjoining Banasandra komatiites (northern extension of Nagamangala belt) and further northwest in Nuggihalli belt and Kalyadi belt we speculate ca. 3.2–3.15 Ga for komatiite eruption in Nagamangala belt. Trace element characteristics particularly HFSE and REE patterns suggest that most of the primary geochemical characteristics are preserved with minor influence of post-magmatic alteration and/or contamination. About 1/3 of studied komatiites show Al-depletion whilst remaining komatiites and komatiite basalts are Al-undepleted. Several samples despite high MgO, (Gd/Yb)_N ratios show low CaO/Al₂O₃ ratios. Such anomalous values could be related to removal of CaO from komatiites during fluid-driven hydrothermal alteration, thus lowering CaO/Al₂O₃ ratios. The elemental characteristics of Al-depleted komatiites such as higher (Gd/Yb)_N (>1.0), CaO/Al₂O₃ (>1.0), Al₂O₃/TiO₂ (<18) together with lower HREE, Y, Zr and Hf indicate their derivation from deeper upper mantle with minor garnet (majorite?) involvement in residue whereas lower (Gd/Yb)_N (<1.0), CaO/Al₂O₃ (<0.9), higher Al₂O₃/TiO₂ (>18) together with higher HREE, Y, Zr suggest their derivation from shallower upper mantle without garnet involvement in residue. The observed chemical characteristics (CaO/Al₂O₃, Al₂O₃/TiO₂, MgO, Ni, Cr, Nb, Zr, Y, Hf, and REE) indicate derivation of the komatiite and komatiite basalt magmas from heterogeneous mantle (depleted to primitive mantle) at different depths in hot spot environments possibly with a rising plume. The low content of incompatible elements in studied komatiites suggest existence of depleted mantle during ca. 3.2 Ga which in turn imply an earlier episode of mantle differentiation, greenstone volcanism and continental growth probably during ca. 3.6–3.3 Ga which is substantiated by Nd and Pb isotope data of gneisses and komatiites in western Dharwar craton (WDC).

© 2013, China University of Geosciences (Beijing) and Peking University. Production and hosting by Elsevier B.V. All rights reserved.

* Corresponding author. Tel.: +91 9560714425.

E-mail addresses: mjayan.geol@gmail.com, mjayananda@rediffmail.com

(M. Jayananda).

Peer-review under responsibility of China University of Geosciences (Beijing).



Production and hosting by Elsevier

1. Introduction

Archaean greenstone belts are dominated by ultramafic-mafic volcanic sequences with minor intermediate to felsic associations. High-Mg volcanic rocks particularly komatiites and komatiitic basalts are more abundant in oldest greenstone sequences and considered to be windows to the Archaean mantle. Komatiites are rare or absent in the Proterozoic and Phanerozoic terrains. Geochemical and isotope signatures of these rocks provide much

insight in understanding the chemical and thermal evolution of Archaean mantle, continental growth rates, secondary processes such as metamorphism and fluid induced alteration. They also provide important constraints on the tectonic context of greenstone volcanism and, degree and depth of melting of mantle. During the last three decades komatiites and komatiite basalts have been extensively studied from the Archaean greenstone belts of southern Africa, Canada, Australia, Brazil, Finland, North China, and India (e.g. Jahn et al., 1982; Gruau et al., 1987; Wilson and Carlson, 1989; Xie et al., 1993, 2012; Arndt, 1994, 2008; Lesher and Arndt, 1995; Fan and Kerrich, 1997; Grove et al., 1997; Parman et al., 1997; Kerrich et al., 1999; Polat et al., 1999; Chavagnac, 2004; Raul Minas and Jost, 2006; Jayananda et al., 2008; Zhai and Santosh, 2011; Dostal and Mueller, 2012; Furnes et al., 2012). The geodynamic context of komatiite magma generation and eruption are still subjects of discussion, whether komatiite magmas are generated by anhydrous melting of deep mantle or wet melting of

shallow mantle (Grove et al., 1997; Parman et al., 1997, 2001; Polat et al., 1999; Arndt, 2003; Chavagnac, 2004). Recently, based on $Fe^{3+}/\Sigma Fe$ ratios of melt inclusions in olivine of komatiites, Berry et al. (2008) have shown anhydrous dry melting of deep mantle generates komatiite magmas during Archaean. Several geodynamic models including oceanic plateaus associated with rising plume, arc setting or combined plume-arc setting have been proposed for the origin of komatiites and komatiitic basalts (De-Witt et al., 1987; Grove et al., 1997; Parman et al., 1997; Polat et al., 1999; Puchtel et al., 1999; Arndt, 2008; Jayananda et al., 2008).

In the Dharwar craton volcano-sedimentary sequences are well preserved in older Sargur Group and younger Dharwar Supergroup (Swaminath and Ramakrishnan, 1981). Several petrologic, geochronologic and geochemical studies focused on the volcanic sequences of Dharwar Supergroup (Balakrishnan et al., 1990, 1999; Zachariah et al., 1995; Anil Kumar et al., 1996; Nutman et al., 1996; Sarma et al., 2008; Anand and Balakrishnan, 2010; Manikyamba

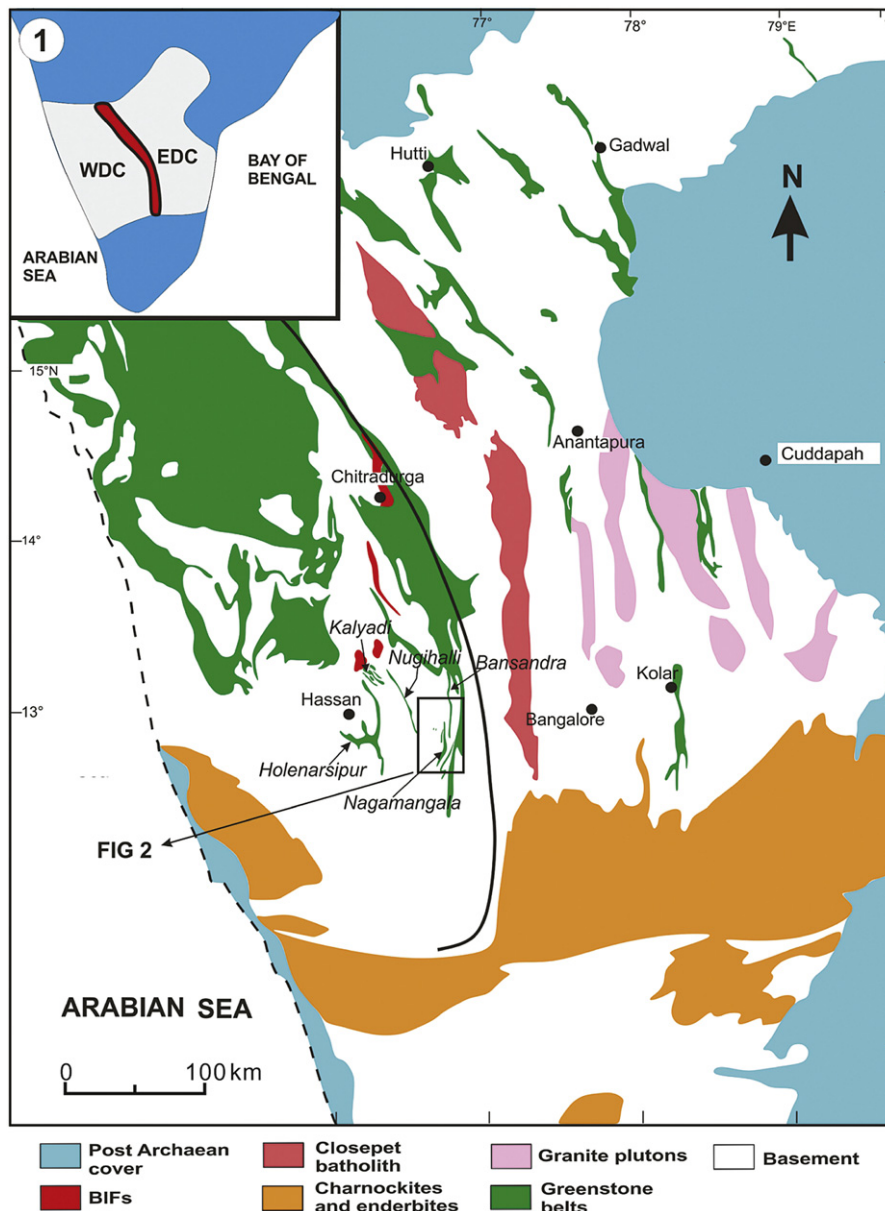


Figure 1. Geological sketch map of the Dharwar craton showing the study area (modified after Chardon et al., 2008).

and Kerrich, 2012), on the other hand no systematic elemental and isotope studies initiated on the Sargur Group volcanic sequences in the western Dharwar craton (WDC). Earlier studies mainly document field, petrographic and major element characteristics for the Sargur Group greenstone sequences in J.C. Pura, Nagamangala, Bansandra, Mayasandra, K.R. Pet and Kalyadi belts (Charan et al., 1988; Srikantia and Venkataramana, 1989; Srikantia and Rao, 1990; Venkata Dasu et al., 1991). On the other hand few geochronologic and geochemical studies initiated on Sargur Group volcanics in the WDC (Peucat et al., 1995; Jayananda et al., 2008; Mondal et al., 2008; Mukherjee et al., 2010). However, no detailed geochemical study initiated on Nagamangala greenstone belt except komatiite documentation by Srikantia and Venkataramana (1989) and Devapriyan et al. (1994). Consequently, the main purpose of this contribution is to present field, petrographic, major and trace elements for the ultramafic to mafic volcanic rocks of Sargur Group Nagamangala greenstone belt to discuss komatiite volcanism, effects of post-magmatic alteration, composition of mantle sources and geodynamic context of magma generation and eruption, Archaean mantle evolution and continental growth connection.

2. Geological and tectonic framework of the Dharwar craton

The Dharwar craton, southern India (Fig. 1) exposes a large tilted section of Archaean continental crust with a progressive transition from upper to lower crustal levels. The craton contains vast areas of 3.36–2.7 Ga TTG gneisses (regionally known as peninsular gneisses), two generations of volcanic-sedimentary sequences (>3.2 Ga Sargur Group and 2.9–2.56 Ga Dharwar Supergroup) and 2.62–2.52 Ga calc-alkaline to potassic granitoids (Chadwick et al., 2000; Jayananda et al., 2000, 2006, 2008; Chardon et al., 2011 for overview). The craton is divided into two sub-blocks western Dharwar craton (WDC) and eastern Dharwar craton (EDC) based on the abundance of the greenstones as well as age of their surrounding basement, crustal thickness, physical conditions of regional metamorphism and degree of melting of the basement (Swaminath et al., 1976; Rollinson et al., 1981; Jayananda et al., 2000; Chardon et al., 2011). The steep mylonitic zone along the eastern boundary of Chitradurga greenstone belt is considered to be the dividing line between these two crustal blocks. The WDC is dominated by older basement (>3.2 Ga TTG with interlayered Sargur Group rocks) which is unconformably overlain by 2.9–2.7 Ga Dharwar Supergroup volcano-sedimentary sequences forming large Bababudan, Chitradurga and Shimoga-Dharwar basins (Meen et al., 1992; Nutman et al., 1992, 1996; Peucat et al., 1993; Jayananda et al., 2008, 2012; Sarma et al., 2011). Few 2.62 Ga high-potassic plutons intrude the TTG basement as well as greenstone sequences mark the cratonization of WDC (Jayananda et al., 2006; Chardon, 2011). On the contrary the EDC comprises younger (2.7–2.6 Ga) grey tonalitic gneisses with large remnants of 3.0–3.32 Ga TTG (Krogstad et al., 1991; Peucat et al., 1993; Nutman et al., 1996; Balakrishnan et al., 1999; Jayananda et al., 2000; Chardon et al., 2002, 2011), thin elongated 2.7–2.56 Ga volcanic-dominated greenstone sequences (Balakrishnan et al., 1990, 1999; Nutman et al., 1996; Sarma et al., 2008; Manikyamba and Kerrich, 2011; Jayananda et al., 2012) and most voluminous north–south trending 2.58–2.52 Ga old calc-alkaline to potassic granitoid intrusions (Krogstad et al., 1991; Jayananda and Peucat, 1995, 2000; Chardon et al., 2002; Moyen et al., 2003; Rogers et al., 2007; Moyen, 2011). The whole Archaean crust in the Dharwar is craton affected by a major high grade metamorphic event close to 2.51 Ga with slow cooling up to 2.45 Ga (Mahabaleshwar et al., 1995; Peucat et al., 1993, 2012; Jayananda and Peucat, 1996) marking the final cratonization.

In the WDC, the Sargur Group volcanic sequences are dominated by ultramafic komatiite and tholeiitic basalts with rare felsic volcanic rocks, whereas the Dharwar Supergroup volcanics contain abundant tholeiitic volcanics with subordinate felsic volcanics. Komatiites and komatiitic basalts are minor or absent in the Dharwar Supergroup greenstone belts. Majority of the earlier studies on the Sargur Group greenstone sequences mainly described either field characteristics including stratigraphic relationships between greenstone belts and surrounding basement or stratigraphy and structure of the greenstone belts (e.g. Viswanatha et al., 1977; Chadwick et al., 1981; Swaminath and Ramakrishnan, 1981; Srikantia and Venkataramana, 1989; Srikantia and Rao, 1990) or document major element characteristics of greenstone volcanics (Venkata Dasu et al., 1991; Devapriyan et al., 1994). Previous geochronological studies on Dharwar Supergroup of the WDC indicate ages of 2911–2720 Ma for the lower Bababudan Group (Anil Kumar et al., 1996; Trendall et al., 1997a) and 2614–2601 Ma for felsic volcanics of upper Chitradurga Group (Nutman et al., 1996; Trendall et al., 1997b). On contrary the Sm-Nd whole rock isochron with combined sample suites of tholeiites and felsic volcanics of upper Chitradurga Group indicate ages of 2740 Ma (Anil Kumar et al., 1996) and amphibolites of adjoining Javagondanahalli belt also indicate 2740 Ma (Jayananda et al., 2011). These ages can be correlated with the ages obtained for the mafic

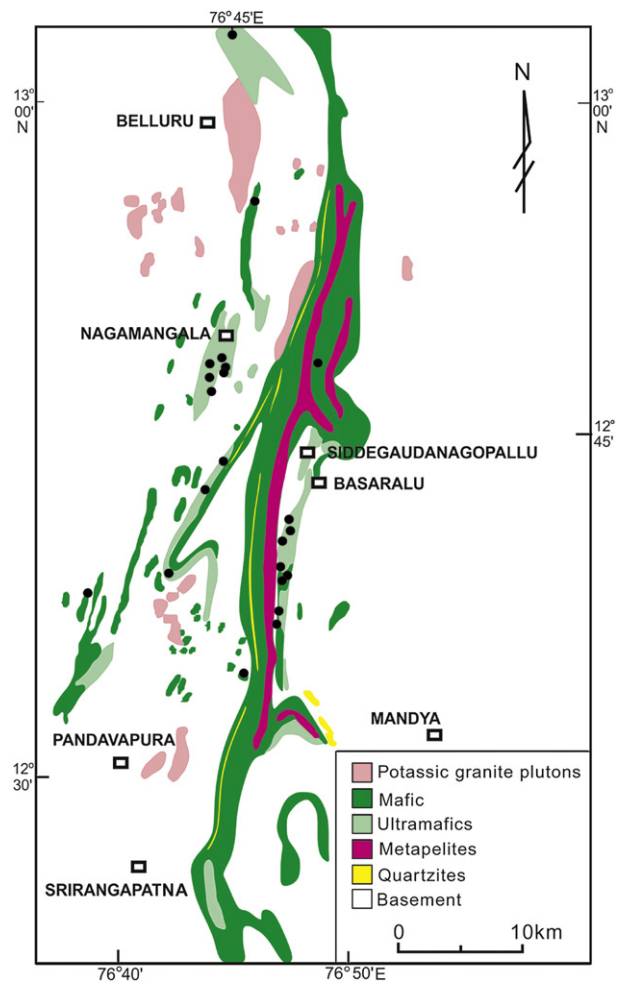


Figure 2. Simplified geological sketch map of the Nagamangala greenstone belt modified after Geological Survey of India resource map (Mandya district) 2000, showing sample locations.

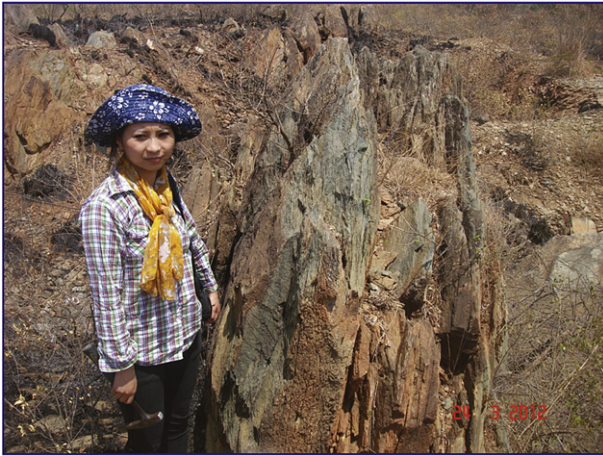


Figure 3. Serpentine-rich komatiite showing steep foliation about 5 km north of Bellur.



Figure 5. Crude pillow structure in ultramafic rock in the southern slope of Honnabetta.

volcanics of the EDC greenstone belts (Balakrishnan et al., 1990, 1999). SHRIMP U-Pb zircon ages together with elemental data characteristics of the EDC greenstone volcanics show two episodes of greenstone volcanism (2.7–2.69 Ga and 2.58–2.54 Ga; Jayananda et al., 2012) in arc-plume environment (Manikyamba et al., 2009).

In the central part of the WDC Sargur Group volcano-sedimentary greenstone sequences are exposed in several greenstone belts, viz. Holenarsipur, Nuggihalli, Kalyadi, Bansandra, J.C. Pura, Krishnarajpet and Nagamangala belts (Fig. 1). The focus of the present work is on ultramafic-mafic volcanic sequence in the Nagamangala greenstone belt.

2.1. Nagamangala greenstone belt

The Sargur Group Nagamangala greenstone belt locates along the western boundary of the Chitradurga greenstone belt (Fig. 2) and extends about 30 km from Nelligere in the north to south of Honakere (Srikantia and Venkataramana, 1989). The greenstone belt is surrounded by 3.3–3.2 Ga TTG basement in the west and 3.2 Ga TTG in the east (Peucat and Jayananda, unpublished data). North–south trending 3.0 Ga old potassic plutons (Jayananda et al., in preparation) show intrusive relationship along western and eastern boundary of the Nagamangala greenstone belt. The

volcanic-sedimentary sequence comprises most abundant ultramafic-mafic association interlayered with sediments such as quartzite and metapelite with minor carbonate and BIFs. The preserved mineral assemblage corresponds to greenschist to lower amphibolite facies conditions of metamorphism (Raase et al., 1986).

Ultramafic rocks comprise massive to schistose, pillowed to spinifex textured komatiites. The different types of ultramafic rocks include medium to fine grained light greyish green serpentine bearing (Fig. 3), whitish green serpentine-tremolite-talc and light green to olive green coloured tremolite-actinolite bearing komatiites. At several localities komatiites show randomly oriented 3–6 cm long amphibole crystals. Devapriyan et al. (1994) interpreted such mesoscopic structures from Honnabetta area as spinifex textures. Those fabrics could be pseudo-spinifex structures developed during post-magmatic hydrothermal alteration processes or metamorphism. Distinct spinifex textured komatiites with criss-crossing sheafs closely spaced parallel blades of olivine (altered to serpentine) ranging from 3 to 7 cm observed at about 1.0 km NW of Siddegoudanakoppalu near Basralu (Fig. 4). Srikantia and Venkataramana (1989) have documented pillow structure in the ultramafic komatiite. In the present study deformed crude pillows observed at few places (Fig. 5). Ultramafic rocks show north trending steep foliation and occasionally display folding. Mafic



Figure 4. Spinifex textured komatiite from 1 km NW of Siddegoudanakoppalu.

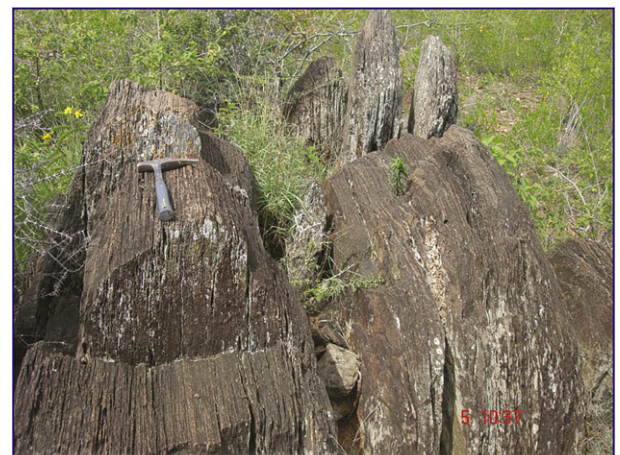


Figure 6. Komatiitic basalt shows steep foliation at Basaralu cross in Nagamangala–Srirangapatna road.

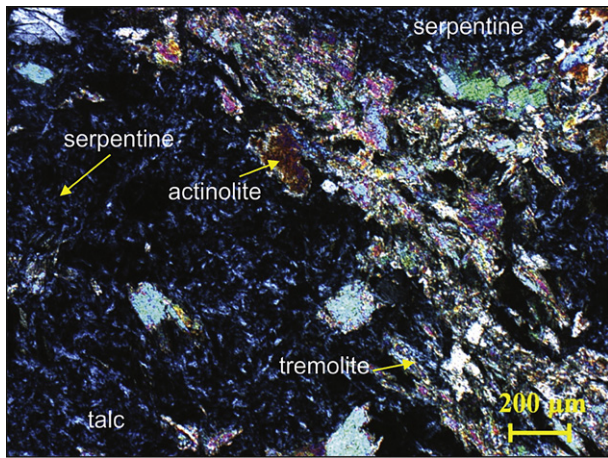


Figure 7. Serpentine-talc-tremolite ± carbonate in komatiite.

rocks are represented by tremolite-actinolite bearing schist, hornblende schist and amphibolite. They occur in association with ultramafic rocks as interlayered sequence but generally confined to higher levels (Devapriyan et al., 1994). They show well developed cleavage with steep dips (Fig. 6). Mafic rocks also show well preserved pillow structures with fine grained chilled margins. Tiny quartz veins measuring 3–4 cm width found along the foliation of the mafic rocks.

3. Petrography

The studied samples show variation in terms of grain size, texture, mineralogy and alteration processes. Textures ranging from spinifex to occasional cumulate textures. The studied rocks do not preserve any primary mineralogy and the observed mineralogy probably developed during hydrothermal alteration processes associated with regional metamorphism (Raase et al., 1986).

The petrographic characteristics of studied ultramafic rocks (komatiites) and mafic rocks (tremolite-actinolite schists) are as follows.

The komatiites show the following assemblages:

Serpentine - talc-tremolite-actinolite ± carbonate (Fig. 7).

Serpentine-tremolite-actinolite ± chlorite (Fig. 8).

Carbonate is a minor phase which occurs as aggregate grains which occasionally forms tiny network of veins. Opaques are not

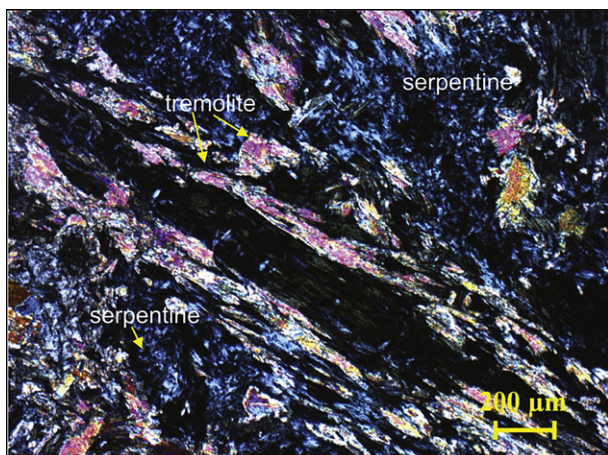


Figure 8. Serpentine-tremolite-actinolite ± chlorite in komatiite.

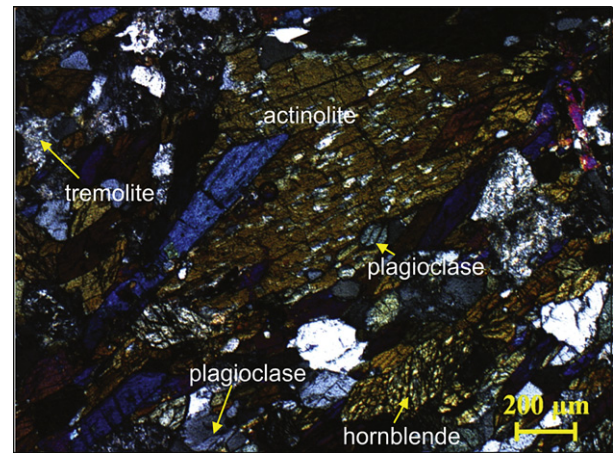


Figure 9. Tremolite-actinolite-minor plagioclase in komatiite basalt.

common and rarely found. Chlorite also found as minor phase in few samples.

The mafic rocks exhibit the following assemblages:

Tremolite-actinolite-minor plagioclase (Fig. 9).

Actinolite-hornblende-plagioclase (Fig. 10).

The preserved mineralogy such as serpentine-talc-tremolite-actinolite-chlorite assemblage together with co-existing actinolite-hornblende suggests greenschist facies to lower amphibolite facies conditions of metamorphism.

4. Geochemistry

4.1. Major and trace elements

Major and trace element compositions of 22 samples presented in Table 1 and analytical procedures are presented in Appendix. The major element oxides used in different plots are on anhydrous basis recalculated to 100. The samples show significant variations in major and trace element contents. The distinction between komatiite and komatiite basalts is based on MgO contents (Arndt and Nisbet, 1982). Most of the analyzed samples are komatiitic in composition with MgO content ranging from 23.17 wt.% to 35.49 wt.% whilst four samples are komatiitic basalt in composition with MgO (9.81 wt.% to 12.48 wt.%). This feature is clearly reflected in Al_2O_3 -($Fe_2O_3 + TiO_2$)-MgO (Fig. 11) triangular diagram (Jensen,

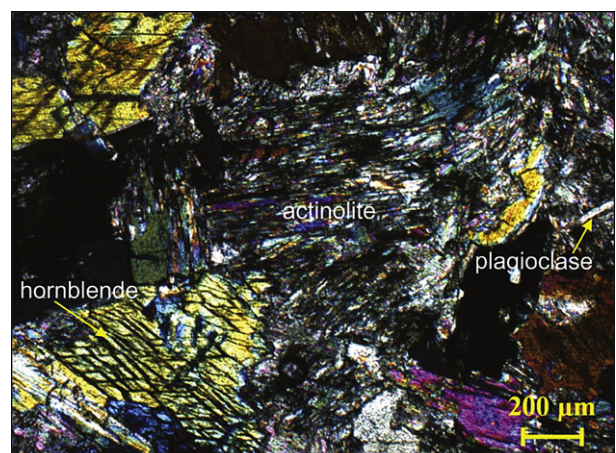


Figure 10. Actinolite-hornblende-plagioclase in komatiite basalt.

Table 1

Major and trace element data for komatiites and komatiite basalt from Sargur Group Nagamangala greenstone belt of western Dharwar craton.

Komatiites																		
Oxides	NBG-10a	NBG11a	NBG12a	NBG12b	NBG-25	NBG-27	NBG-16	NM-03	NM-04	NM-05	NM-12	NM15a	NM-15b	NM-16	NM-17	NM1	NM2	NM3
SiO ₂	40.47	43.52	42.96	43.42	42.36	43.51	41.24	43.45	43.93	42.58	43.46	43.64	41.82	42.77	42.91	46.9	45.09	41.81
TiO ₂	0.29	0.28	0.28	0.33	0.35	0.36	0.28	0.27	0.26	0.22	0.35	0.29	0.26	0.34	0.29	0.29	0.23	0.36
Al ₂ O ₃	3.87	3.79	3.94	5.13	5.16	4.31	4.15	5.32	5.19	3.71	3.98	3.73	3.95	4.08	4.58	4.65	4.42	4.21
Fe ₂ O ₃	7.83	8.07	8.53	9.21	9.03	10.80	8.11	9.03	8.53	6.90	8.62	7.96	7.38	8.91	9.40	9.6	9.03	9.01
MnO	0.19	0.16	0.18	0.19	0.40	0.19	0.16	0.18	0.16	0.17	0.02	0.15	0.17	0.19	0.14	0.23	0.1	0.03
MgO	33.13	32.61	30.52	29.02	30.17	28.85	34.73	29.31	31.12	34.87	32.98	32.62	35.79	31.87	30.89	27.17	30.66	33.87
CaO	4.35	4.04	4.65	5.03	4.26	4.38	3.57	3.55	3.70	3.98	3.30	2.96	3.56	3.91	4.18	4.95	4.27	4.89
Na ₂ O	2.40	0.37	0.41	0.14	0.23	0.25	0.35	0.35	0.26	0.30	0.33	0.18	0.19	0.30	0.19	0.5	0.29	0.01
K ₂ O	0.23	0.04	0.04	0.08	0.06	0.04	0.04	0.04	0.04	0.05	0.04	0.02	0.03	0.05	0.03	0.03	0.01	0.01
P ₂ O ₅	0.09	0.01	0.03	0.03	0.05	0.02	0.01	0.03	0.04	0.11	0.02	0.02	0.02	0.03	0.02	0.04	0.01	0.04
LOI	7.12	6.63	7.54	7.21	8.43	6.98	6.79	6.49	5.89	6.74	6.61	7.93	6.81	6.93	6.87	5.77	5.5	4.98
Total	99.97	99.52	99.08	99.79	100.50	99.69	99.43	98.02	99.12	99.63	99.71	99.50	99.98	99.38	99.50	100.13	99.61	99.22
Ba	15.82	31.68	16.48	73.43	24.87	26.88	30.52	3.29	6.57	2.87	1.90	29.37	29.36	23.34	2.89			
Cr	1844.6	3288.8	3859.9	2358.9	1464.2	2314.7	3353.9	2516.4	3565.3	1490.0	1293.8	2978.5	2976.1	2083.0	2130.7			
Nb	1.68	1.20	1.20	1.59	1.51	1.34	1.23	1.18	1.35	1.26	1.28	1.27	1.16	1.22	1.10			
Ni	1137.9	1315.9	1492.2	1349.5	1250	1512.5	1298.6	1589.8	1566.4	1331.2	1231.2	1220.1	1286.1	1120.7	1438.2			
Rb	1.83	1.52	1.66	1.70	6.99	4.84	1.80	0.40	0.83	0.43	0.51	1.94	1.23	2.33	0.35			
Sr	61.03	15.95	18.12	52.04	62.02	86.10	15.32	14.44	25.20	12.92	7.62	24.56	7.66	30.96	16.21			
V	247.02	126.27	222.82	181.79	469.78	259.06	132.15	96.25	117.78	54.68	30.08	181.80	162.48	162.30	85.37			
Y	15.99	6.40	10.33	10.85	35.73	11.67	5.35	4.00	7.73	7.52	4.67	6.97	6.00	11.12	3.49			
Zn	67.79	57.69	123.48	63.20	259.05	86.91	86.42	60.96	166.55	60.83	51.76	91.75	86.83	68.92	46.95			
Zr	12.69	12.63	18.96	15.65	14.09	11.13	14.84	16.59	22.91	20.09	13.14	15.63	9.58	10.98	6.98			
Th	0.15	0.39	0.35	0.57	0.74	0.43	0.45	0.30	0.34	0.38	0.14	0.55	0.38	0.51	0.12			
U	0.02	0.03	0.02	0.05	0.03	0.02	0.03	0.02	0.02	0.01	0.05	0.03	0.02	0.02	0.03			
Hf	0.04	0.04	0.04	0.04	0.04	0.05	0.05	0.05	0.04	0.04	0.04	0.05	0.05	0.05	0.04			
Pb	0.61	0.63	0.94	1.52	1.18	0.81	0.68	0.53	0.87	0.84	0.66	0.76	0.59	0.69	0.50			
Ti	4855.95	4076.60	3477.10	3776.85	4385.6	3297.2	4556.2	4316.4	4136.5	2757.7	3297.2	4376.3	3956.7	4177.3	2016.1			
La	1.75	1.08	1.69	2.66	4.53	1.92	2.02	1.34	1.59	2.19	1.48	1.81	1.00	1.85	1.22			
Sc	31.09	25.26	38.60	34.08	41.29	28.05	27.21	23.77	16.63	16.68	10.07	23.44	28.56	31.02	16.52			
Co	25.08	82.36	97.24	45.64	47.13	88.58	80.77	55.96	99.29	43.25	43.68	88.97	88.63	82.43	56.28			
Cu	113.38	19.21	23.87	26.02	51.89	125.85	21.86	20.71	24.93	19.77	14.02	43.91	21.25	33.46	46.34			
Ga	4.99	8.46	11.68	11.12	26.25	14.15	8.61	4.51	9.06	2.64	4.03	10.35	11.55	9.67	4.59			
Ta	0.16	0.10	0.09	0.14	0.24	0.09	0.07	0.04	0.11	0.11	0.07	0.21	0.06	0.09	0.08			
Pr	0.64	0.31	0.55	0.65	2.26	0.67	0.56	0.42	0.64	0.92	0.44	0.48	0.31	0.63	0.31			
Nd	4.26	1.42	2.78	3.73	11.11	3.49	2.38	1.82	3.06	4.13	1.29	2.05	1.39	3.08	1.64			
Sm	1.33	0.42	0.93	1.00	2.63	1.31	0.57	0.47	0.84	1.01	0.56	0.55	0.44	0.60	0.27			
Eu	0.49	0.14	0.26	0.41	0.41	0.56	0.16	0.14	0.34	0.17	0.24	0.11	0.15	0.30	0.20			
Gd	2.10	0.60	1.11	1.42	4.50	1.92	0.67	0.53	1.06	1.18	0.69	0.85	0.56	1.25	0.62			
Tb	0.39	0.13	0.24	0.26	0.89	0.34	0.12	0.10	0.19	0.20	0.13	0.16	0.12	0.25	0.07			
Dy	2.26	0.85	1.45	1.56	5.37	1.95	0.73	0.59	1.16	1.16	0.77	1.02	0.82	1.56	0.51			
Ho	0.52	0.23	0.38	0.34	1.32	0.45	0.18	0.14	0.28	0.27	0.17	0.25	0.20	0.40	0.13			
Er	1.70	0.71	1.17	1.18	3.89	1.22	0.62	0.43	0.79	0.81	0.45	0.81	0.67	1.27	0.38			
Tm	0.28	0.13	0.19	0.20	0.65	0.21	0.12	0.08	0.14	0.13	0.07	0.15	0.13	0.24	0.07			
Yb	1.51	0.80	1.19	1.13	3.62	1.12	0.72	0.46	0.83	0.66	0.38	0.87	0.76	1.35	0.40			
Lu	0.23	0.13	0.19	0.19	0.60	0.18	0.13	0.08	0.13	0.11	0.05	0.16	0.13	0.23	0.06			
ΣREE	22.26	9.16	16.11	20.48	19.53	13.05	58.99	9.62	15.24	18.16	3.71	12.76	8.77	17.91	6.95			
Fe ₂ O ₃ /(Fe ₂ O ₃ + MgO)	0.19	0.20	0.22	0.24	0.23	0.27	0.19	0.24	0.22	0.17	0.21	0.20	0.17	0.22	0.23	0.26	0.23	0.21
FeO/(FeO + MgO)	0.17	0.18	0.20	0.22	0.21	0.25	0.17	0.21	0.20	0.15	0.19	0.18	0.15	0.20	0.21	0.23	0.21	0.19
CaO/Al ₂ O ₃	1.12	1.07	1.18	0.98	0.83	1.02	0.86	0.67	0.71	1.07	0.83	0.79	0.90	0.96	0.91	1.06	0.97	1.16
Al ₂ O ₃ /TiO ₂	13.34	13.54	14.07	15.55	14.74	11.97	14.82	19.70	19.96	16.86	11.37	12.86	15.19	12	15.79	16.03	19.22	11.69
(Gd/Yb) _N	1.15	0.62	0.77	1.04	1.03	1.42	0.76	0.95	1.06	1.48	1.50	0.82	0.60	0.77	1.28			
Nb/Th	3.93	3.96	3.31	9.11	2.32	3.10	2.37	8.39	10.92	3.10	3.41	2.80	2.05	3.11	2.71			
Nb/U	73.19	92.35	24.54	49.84	74.97	59.71	42.19	83.27	46.45	49.18	29.81	53.09	57.26	42.53	73.75			
Nb/La	0.85	0.57	0.86	0.70	1.16	0.66	0.90	0.96	1.12	0.71	0.60	0.33	0.70	0.61	0.88			
Ti/Zr	108.26	82.30	150.43	167.86	247.55	228.00	173.24	229.42	193.56	109.97	144.69	186.64	177.62	184.02	156.00			
Eu/Eu*	0.18	0.15	0.14	0.17	0.06	0.23	0.11	0.13	0.17	0.07	0.26	0.08	0.16	0.16	0.20			
Ce/Ce*	1.11	0.92	1.01	1.04	0.90	0.93	1.11	0.97	1.02	0.80	0.43	0.90	0.92	1.11	0.21			

Komatiite basalt					
Oxides	NM11b	NM14	NBG13	NBG21	
SiO ₂	48.72	48.35	50.93	49.05	
TiO ₂	0.62	0.46	0.51	0.57	
Al ₂ O ₃	8.97	8.92	9.55	9.93	
Fe ₂ O ₃	13.18	12.86	12.31	13.19	
MnO	0.22	0.19	0.15	0.20	
MgO	11.76	12.48	9.81	9.88	
CaO	8.34	8.02	8.18	9.03	
Na ₂ O	1.64	2.46	2.71	1.35	
K ₂ O	0.59	0.19	0.74	0.23	
P ₂ O ₅	0.16	0.12	0.30	0.08	
LOI	4.39	5.06	4.70	5.10	
Total	98.59	99.11	99.89	98.61	
Ba	33.55	35.64	60.96	33.96	
Cr	48.38	52.92	160.55	176.05	
Nb	6.63	4.06	5.51	1.73	
Ni	23.87	28.34	80.54	71.71	
Rb	9.61	3.94	4.61	2.78	
Sr	119.86	98.59	158.32	105.11	
V	383.46	437.30	283.26	233.54	
Y	39.29	30.76	32.66	12.61	
Zn	87.21	68.62	78.67	70.76	
Zr	20.40	26.13	17.48	15.46	
Th	0.51	0.35	0.77	0.24	
U	0.58	0.54	0.87	0.25	
Hf	0.04	0.09	0.05	0.06	
Pb	0.97	0.62	1.39	1.04	
Ti	2218.15	1918.40	2457.95	2817.65	
La	5.23	4.10	12.04	3.00	
Sc	45.48	45.15	40.94	40.30	
Co	33.03	29.55	33.01	28.26	
Cu	60.31	248.73	147.10	35.44	
Ga	7.21	6.12	7.20	6.45	
Ta	0.63	0.38	0.50	0.15	
Pr	1.53	1.31	3.19	0.90	
Nd	9.58	8.80	18.92	5.52	
Sm	3.31	2.68	4.85	1.65	
Eu	1.14	1.00	1.40	0.54	
Gd	5.00	3.95	6.13	2.28	
Tb	0.96	0.74	0.95	0.39	
Dy	5.61	4.32	4.97	2.11	
Ho	1.24	0.96	1.03	0.42	
Er	4.06	3.21	3.35	1.32	
Tm	0.69	0.54	0.58	0.21	
Yb	3.91	3.07	3.07	1.05	
Lu	0.61	0.49	0.46	0.15	
ΣREE	88.29	25.99	53.09	44.47	
Fe ₂ O ₃ /(Fe ₂ O ₃ + MgO)	0.53	0.51	0.56	0.57	
FeO/(FeO + MgO)	0.50	0.48	0.53	0.54	
CaO/Al ₂ O ₃	0.93	0.90	0.86	0.91	
Al ₂ O ₃ /TiO ₂	14.47	19.39	18.73	17.42	
Gd/Yb	1.06	1.07	1.65	1.80	
Nb/Th	7.17	7.19	13.07	11.47	
Nb/U	6.35	6.85	11.37	7.58	
Nb/La	0.46	0.58	1.27	0.99	
Ti/Zr	84.32	109.24	65.19	44.02	
Eu/Eu*	0.18	0.17	0.12	0.15	
Ce/Ce*	0.88	0.98	1.06	0.96	

Eu/Eu* = 2Eu_N/(Sm+Gd)_N
Ce/Ce* = 2Ce_N/(La+Pr)_N

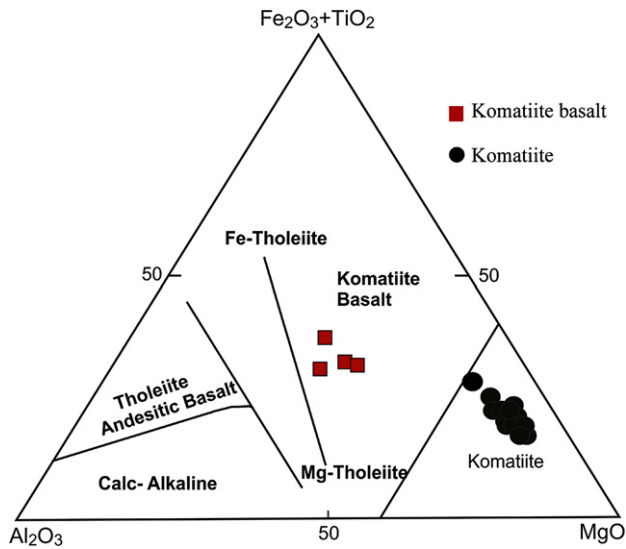


Figure 11. Al_2O_3 -($\text{Fe}_2\text{O}_3 + \text{TiO}_2$)- MgO triangular plot (Jensen, 1976 modified by Viljoen et al., 1982).

1976 as modified by Viljoen et al., 1982) and CaO - MgO - Al_2O_3 (Fig. 12) of Viljoen et al. (1982). On AFM diagram (Irvine and Baragar, 1971) komatiites define classical komatiite trend whilst komatiite basalts show tholeiite trend (Fig. 13). Among the analyzed komatiites seven samples belong to Al-depleted Barberton-type showing $\text{CaO}/\text{Al}_2\text{O}_3$ ratios between 1.02 and 1.18 and $\text{Al}_2\text{O}_3/\text{TiO}_2$ ratios (11.69–16.86) whilst the remaining samples show transitional characteristics of both Al-depleted and Al-undepleted nature with $\text{CaO}/\text{Al}_2\text{O}_3$ ratios between 0.67 and 0.98 and $\text{Al}_2\text{O}_3/\text{TiO}_2$ ratios (11.37–19.70). Similarly, komatiite basalt also shows transitional characteristics of both Al-depleted Barberton-type and Al-undepleted Munro-type with $\text{CaO}/\text{Al}_2\text{O}_3$ ratios between 0.8 and 0.9 and $\text{Al}_2\text{O}_3/\text{TiO}_2$ ratios (14.47–19.39). On the Harker's binary diagrams major elements versus MgO , majority of major element oxides form two clusters of komatiite and komatiite basalt but together define moderate trends for some major element oxides (Fig. 14). Al_2O_3 , SiO_2 , Fe_2O_3 , CaO and P_2O_5 exhibit moderate negative correlation with MgO whilst TiO_2 and alkalis do not define any trend (see Fig. 14).

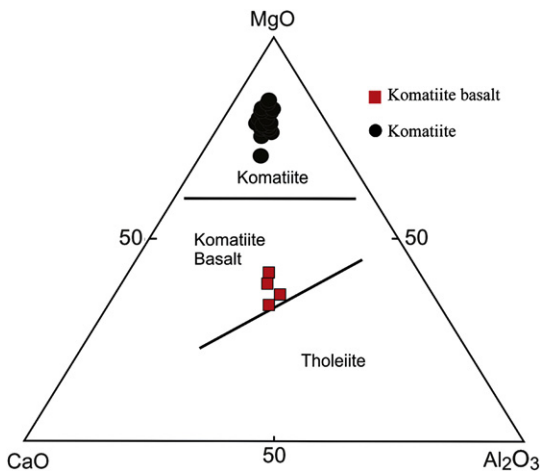


Figure 12. CaO - MgO - Al_2O_3 Jensen cation diagram after Jensen (1976), modified by Viljoen et al. (1982).

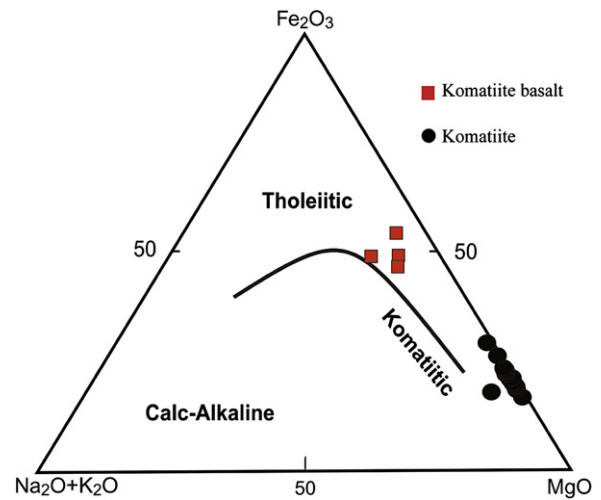


Figure 13. AFM diagram after Irvine and Baragar (1971).

The studied komatiites and komatiite basalts show large variation in trace element contents. On Harker's binary diagrams they form clustering for komatiites and komatiite basalts. Only Ni and Cr show positive correlation with MgO whilst Zr, Nd and Yb show moderate negative correlation (Fig. 15). Other trace elements such as Ba, Rb and Zn show scattering. Trends observed for Ni and Cr could be related to olivine fractionation whilst scattering of Rb and Ba could be due to post-magmatic alteration processes.

4.2. Rare earth elements (REE)

REE are normalised to ordinary chondrites and divided by 1.2 with values of Pr, Tb, Ho and Tm are interpolated after Taylor and Gordon (1977). All the samples of the studied komatiites and komatiite basalts show large variation in REE contents. The komatiites exhibit total REE content ranging from 3.71 to 58.99 ppm. The komatiite basalts display significant variation in REE but generally show higher total REE (26–88 ppm) compared to komatiites. The komatiites are divided into three groups based on total REE, shape of the patterns and Eu anomalies. Group I komatiites are characterized by low to moderate total REE (8.77–22.26 ppm) and show flat REE patterns with $(\text{Gd}/\text{Yb})_N$ ratios (0.62–1.42) except few samples which show either slight depletion or enrichment in MREE (Fig. 16a). The second group is also characterized by moderate total REE (12.75–18.16 ppm), flat REE patterns with $(\text{Gd}/\text{Yb})_N$ ratios of 0.81–1.48 and shows negative Eu anomalies (Fig. 16b). Group III komatiites are characterized by low total REE (3.71–6.94 ppm) with $(\text{Gd}/\text{Yb})_N$ values (1.28–1.50) and slightly enriched MREE compared to LREE (Fig. 16c).

The komatiite basalts show distinct REE patterns. Among the four analyzed samples, sample NBG21 shows low REE and REE pattern is characterized by flat LREE with slight HREE fractionation whilst two samples (NM11b and NM14) show chondritic LREE with HREE enrichment (Fig. 17). On the contrary the sample NBG13 shows higher total REE with LREE enrichment and HREE fractionation.

The primitive mantle (Sun and McDonough, 1989) normalised multi-element patterns of the komatiites displays variable anomalies of LIL and HFS elements.

Group I komatiites show crossing of LIL elements with negative U and positive Pb anomalies, strong negative Hf anomalies and flat HREE including Y (Fig. 18a). Nb shows either positive or no significant anomalies except one sample that shows negative

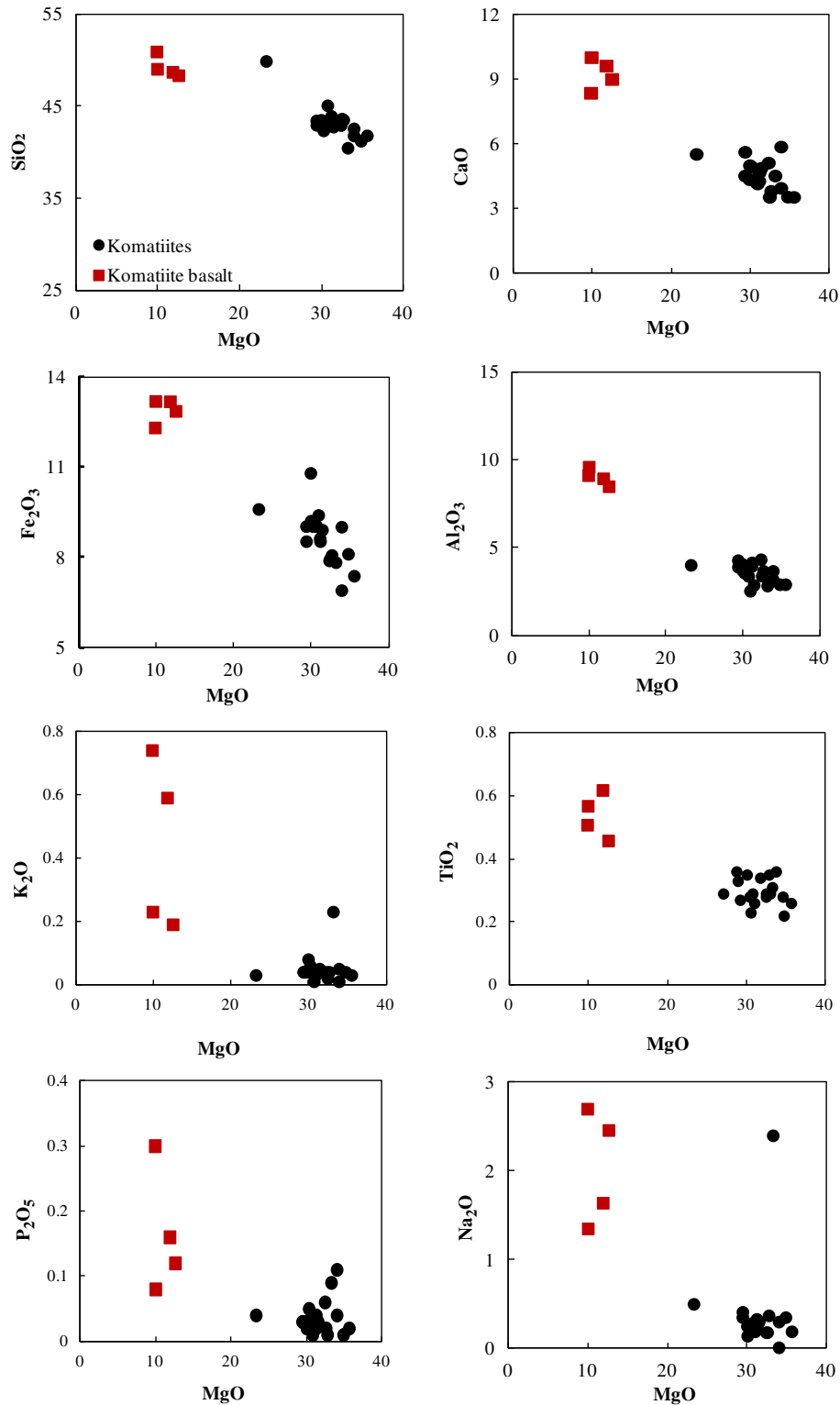


Figure 14. Harker's binary diagram showing selected major oxides versus MgO.

anomaly whilst Sr shows either negative or no anomaly except one sample showing positive anomaly. Group II komatiites show similar patterns to Group I with slight negative Eu anomalies and without significant Nb anomalies (Fig. 18b). Group III komatiites show relatively smooth patterns without any crossing of LILE, with positive or without Nb anomalies (Fig. 18c). They are also

characterized by positive Ti anomalies and strong negative Hf anomalies.

On the primitive mantle-normalised multi-element patterns, four komatiite basalts show relatively uniform Ti, Zr, and LREE without significant Nb anomalies and show strong negative Hf anomalies and flat HREE (Fig. 19). They also show negative Ce, Sr and Eu anomalies.

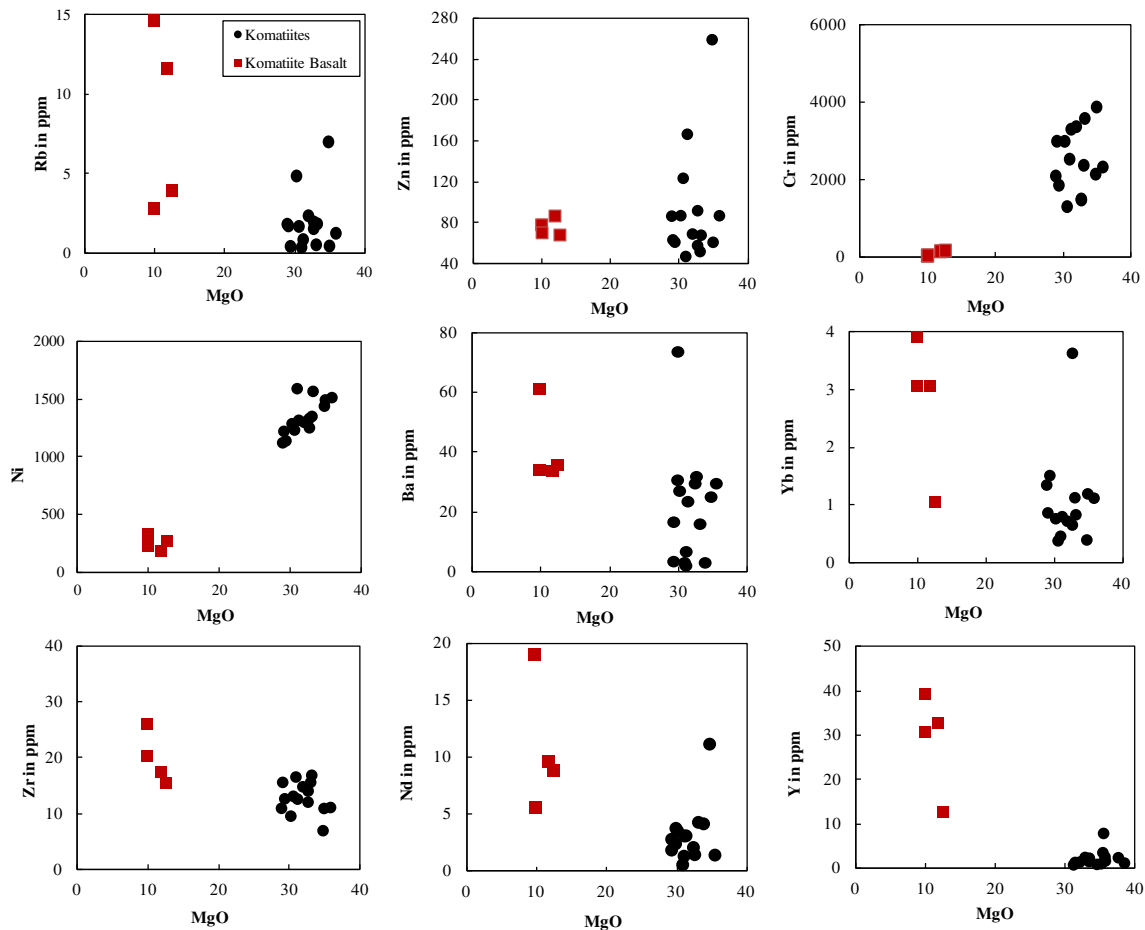


Figure 15. Harker's variation diagrams for selected trace elements plotted against MgO.

5. Discussion

5.1. Timing of komatiite volcanism in Nagamangala greenstone belt

In recent years Sm-Nd and Pb-Pb whole rock isochron ages (Table 2) presented for the komatiites from WDC (Jayananda et al., 2008; Mondal et al., 2008; Maya et al., 2011). In this contribution we do not present Sm-Nd isotope data but we discuss qualitatively the possible time framework of komatiite volcanism in the Nagamangala greenstone belt with respect to timing of surrounding TTG basement considering the isotopic age data presented for komatiites of neighbouring greenstone belts and adjoining TTG. A 16 point Sm-Nd whole rock isochron including the J.C. Pura, Bansandra, Kalyadi and Nuggihalli belts defines an age of 3552 ± 110 Ma for komatiite volcanism in the central part of the western Dharwar craton (Jayananda et al., 2008) which is attributed to the eruption of different komatiites within a short time interval with close initial Nd isotopic compositions. Six samples of the J.C. Pura komatiites yield Sm-Nd whole rock isochron age of 3384 ± 200 Ma whilst the surrounding TTG gneiss indicates SHRIMP U-Pb zircon age of 3315 ± 5 Ma (Chardon, 1997). Komatiites of Kalyadi and Nuggihalli together define an isochron age of 3284 ± 310 Ma (Jayananda et al., 2008). Recently, Maya et al. (2011) presented ^{147}Sm - ^{143}Nd whole rock isochron age of 3136 ± 200 Ma for the komatiite suite of Bansandra greenstone belt which forms northern extension of Nagamangala belt (about 40 km north of the present study). Zircons in the gneisses from northwest of Bansandra belt provide U-Pb zircon ages of 3167–3127 Ma (Chardon, 1997). The ultramafic - mafic sequences of

Nuggihalli greenstone belt from the northwest of studied area indicate Pb-Pb whole rock isochron age of 3156 ± 170 Ma (Mondal et al., 2008) whereas the surrounding gneisses provide U-Pb zircon ages close to 3100 Ma (Bidyananda et al., 2003). The above lines of evidences show extensive greenstone volcanism during 3.35–3.15 Ga which is sub-contemporaneous with accretion of surrounding TTG. Considering the published ages of Bansandra greenstone belt and Nuggihalli-Kalyadi belt located close proximity, we speculate that the time framework of komatiite volcanism in the Nagamangala belt probably occurred between 3.2 and 3.15 Ga.

5.2. Post-magmatic processes: alteration and metamorphism

Geochemical (major and trace elements) and Nd isotope studies conducted on the Archaean komatiites across the world show that mobility of LILE and REE in most cases is controlled by secondary processes such as metamorphism or fluid induced hydrothermal alteration processes (Arndt et al., 1989; Tourpin et al., 1991; Gruau et al., 1992; Chavagnac, 2004). The detailed geochemical study of REE during fluid-rock interaction has shown that mobility of these elements are enhanced by their ability to form complex with F and/or CO_2 dominated fluid phases (Bau, 1981). Recent petrologic, geochemical and Nd isotope studies (Jayananda et al., 2008) have shown that komatiites in the WDC were not affected by large-scale alteration processes and preserve original REE and Nd isotope signatures. The komatiites and komatiite basalts of Nagamangala greenstone belt are affected by hydrothermal alteration and greenschist to lower amphibolite facies metamorphism (Raase

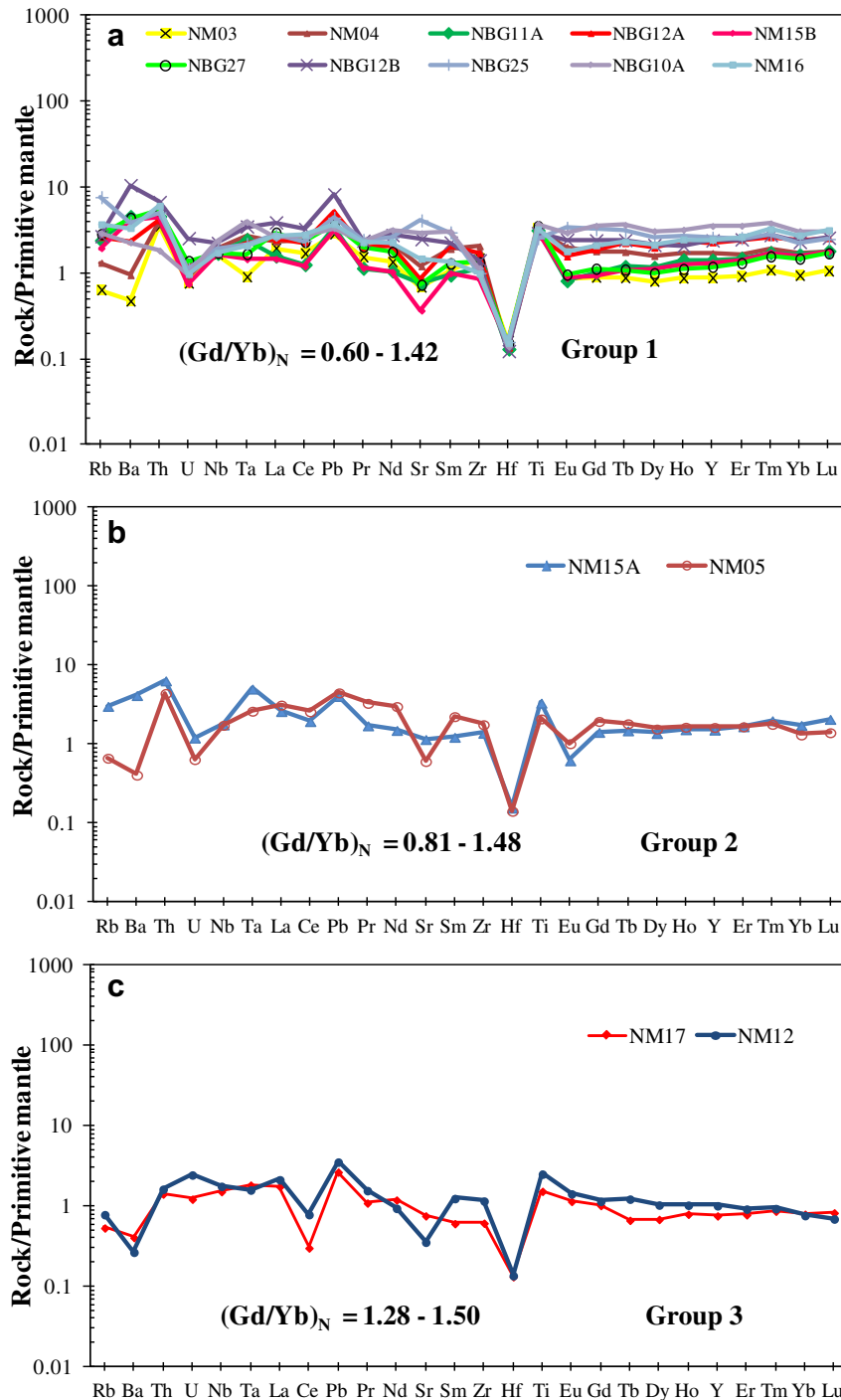


Figure 16. Chondrite normalised REE patterns of Komatiites of Nagamangala greenstone belt.

et al., 1986). The preserved mineralogy such as serpentine, talc, tremolite, actinolite, and chlorite indicates recrystallization under low-grade conditions. Presence of occasional carbonate can be attributed to CO₂-rich fluid induced alteration processes. In this study we use relatively immobile elements (HFSE and REE) for discussion of petrogenetic processes particularly characterizing the source composition. Most of the analyzed samples show uniform Al₂O₃/TiO₂ ratios with relatively smooth REE patterns. On the other hand primitive mantle-normalised multi-element diagram shows crossing of LILE indicating their mobility, whilst HFSE and REE rule out the possibility of large-scale secondary alteration processes.

Further, smooth fractionated trends of Al₂O₃, Fe₂O₃, CaO, and P₂O₅ against MgO preclude any large-scale alteration process. Komatiites show negative Ce anomalies (see Fig. 18a–c) whilst one komatiite basalt shows positive Ce anomaly. Several studies have shown that Ce anomalies occur in response to oxidation of Ce³⁺ to Ce⁴⁺ and precipitation of Ce⁴⁺ from solution as CeO₂ (e.g. Braun et al., 1993). The depletion of Ce and resultant negative Ce anomalies could be attributed to removal of Ce by circulating fluids during metamorphism. Indeed Nagamangala greenstone belt is affected by shear deformation and fluid flow associated with metamorphism as indicated by quartz veins and tiny carbonate vein network. The

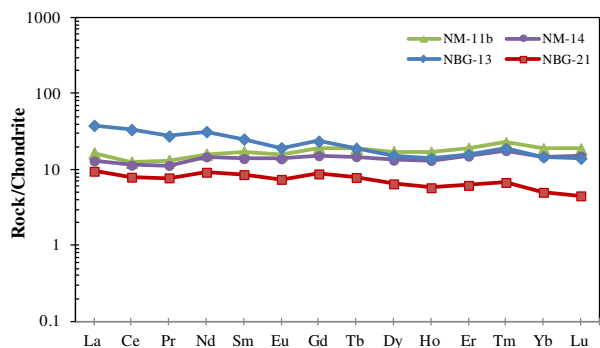


Figure 17. Chondrite normalised REE patterns of komatiite basalts of Nagamangala.

positive Ce anomaly observed could be probably related to precipitation of Ce by circulation of fluid phase in an oxidizing environment. Two samples despite high MgO contents show negative Eu anomalies implying removal of Eu probably during hydrothermal alteration process. Eu anomalies are also observed in the komatiites of other cratons, which are generally attributed to secondary alteration processes (Sun and Nesbitt, 1978; Ludden et al., 1982; Arndt, 1994). On the Ti/Zr versus $\text{Al}_2\text{O}_3/\text{TiO}_2$ diagram majority of the samples form cluster between Primitive mantle and MORB and do not show scattering, precluding influence of fluid induced alteration processes (Fig. 20). Published isotopic age data (Peucat et al., 1993, 2012; Jayananda and Peucat, 1996; Jayananda et al., 2006) indicate that WDC is affected by at least three major thermal events close to 3.0 Ga, 2.62 Ga and 2.5 Ga as indicated by the Pb-loss in zircons and also emplacement of potassic granites. Fluids associated with these thermal events probably caused the mobility of LIL elements. In summary the studied komatiites and komatiitic basalts were not affected by large-scale alteration processes and chemistry of these rocks can be used to constrain Archaean mantle.

5.3. Crustal contamination

The continental crust is enriched in incompatible elements (high LREE and HFSE) compared to mantle. The upward movement of komatiite magmas through continental lithosphere to the surface makes crustal contamination possible. Field evidences such as pillow structure indicate eruption in marine environment. Majority of the studied komatiites do not show LREE enrichment, negative Nb anomalies on the primitive mantle-normalised diagrams which do not show significant crustal contamination. In addition most of the studied komatiites are also characterized by relatively high Zr/Th (28–93) in the range of primitive mantle, except four samples close to continental crust (Zr/Th ~20). This argues against incorporation of large amount of old continental crust into the komatiite magma during their ascent. This argument is also supported by Ti/Zr, Nb/U, Nb/Th, Nb/La ratios which are close to the recommended values for mantle (Hofmann, 1988). Consequently it seems unlikely that crustal contamination is responsible for chemical characteristics of Nagamangala komatiites.

5.4. Magmatic differentiation

The analyzed samples are mainly komatiitic and only four samples are komatiitic basalts in composition. They form two clusters on binary diagrams and do not define linear trends for major and trace elements indicating that these magmas were not evolved by differentiation of single parental magma but two magmas probably derived from different depths and evolved

independently. Negative trends of Al_2O_3 , Fe_2O_3 , CaO, TiO_2 , SiO_2 and P_2O_5 against MgO suggest olivine fractionation (see Fig. 14). Further, the strong positive correlation of Ni, Cr with MgO but negative correlation with Al_2O_3 and TiO_2 can be attributed to fractionation of olivine. The moderate negative correlation of Zr, Y and Yb indicates possible garnet involvement as fractionating phase.

5.5. Nature and composition of mantle sources

5.5.1. Al-depletion in komatiites

Based on Al-contents two major types of komatiites have been recognized viz. Al-depleted and Al-undepleted (Nesbitt and Sun, 1976; Sun, 1984). Further, Arndt (2003) has classified komatiites Al-depleted Barberton-type and Al-undepleted Munro-type. The Barberton-type komatiites are characterized by high $\text{CaO}/\text{Al}_2\text{O}_3$ (>1.0) and low $\text{Al}_2\text{O}_3/\text{TiO}_2$ (<16) which are common in the oldest (>3.3 Ga) greenstone sequences. On the contrary the Munro-type komatiites exhibit lower $\text{CaO}/\text{Al}_2\text{O}_3$ (<1.0) and higher $\text{Al}_2\text{O}_3/\text{TiO}_2$ (>20) which are mainly confined to younger (~2.7 Ga) greenstone successions and also found in Proterozoic and Phanerozoic plateaus (Kerr et al., 1996). The Al-depleted and Al-undepleted nature reflects essentially anhydrous melting of hot mantle at different depths (Arndt, 2008). The Al-depleted komatiites are explained by melting of mantle at greater depth in the presence of residual garnet. At relatively shallower depth garnet melts near peridotite-solidus and removed from the residue before melts acquire komatiitic composition which results in the formation of Al-undepleted komatiite (Arndt, 2003). Experimental studies (Ohtani et al., 1989; Herzberg, 1999) have shown that Al-depleted komatiites are generated by partial melting of peridotite at pressures greater than 8 GPa, whilst Al-undepleted komatiites have been explained by high degree melting of peridotite at shallow level in mantle. Further, Jahn et al. (1982) and Gruau et al. (1992) have used $\text{CaO}/\text{Al}_2\text{O}_3$ ratios and $(\text{Gd}/\text{Yb})_N$ values to constrain source characteristics of mantle sources particularly role garnet fractionation, where high $\text{CaO}/\text{Al}_2\text{O}_3$ ratios (>1.0) and $(\text{Gd}/\text{Yb})_N$ (>1.0) are invoked to the presence of garnet as residual phase in the mantle whilst low $\text{CaO}/\text{Al}_2\text{O}_3$ ratios (<1.0) and $(\text{Gd}/\text{Yb})_N$ (<1.0) have been attributed to garnet melting.

In the present study about 1/3 of the analyzed komatiites and komatiite basalts samples show Al-depletion ($\text{CaO}/\text{Al}_2\text{O}_3 > 1.0$, $\text{Al}_2\text{O}_3/\text{TiO}_2 \leq 18$) implying involvement of garnet in residue of mantle source while remaining samples generally show lower $\text{CaO}/\text{Al}_2\text{O}_3$ (>1.0) and higher $\text{Al}_2\text{O}_3/\text{TiO}_2$ (>20) suggesting garnet melting during generation of komatiite magma. Major element ratios in combination of $(\text{Gd}/\text{Yb})_N$ ratios have been used to characterize sources (Jahn et al., 1982; Arndt, 2003). Five samples despite their high $(\text{Gd}/\text{Yb})_N$ ratios and MgO contents (>30 wt.%) show low $\text{CaO}/\text{Al}_2\text{O}_3$ ratios (<1.0). On the other hand two komatiite basalts show slightly higher $\text{CaO}/\text{Al}_2\text{O}_3$ values despite low MgO contents. Chikhaoui (1981) has explained that CaO content in volcanic rocks is generally reduced by hydrous alteration causing the lowering of $\text{CaO}/\text{Al}_2\text{O}_3$ ratios. Such mechanisms of post-magmatic hydrothermal alteration of komatiites can explain the observed values of lower $\text{CaO}/\text{Al}_2\text{O}_3$ ratios despite high MgO (>30 wt.%), low $\text{Al}_2\text{O}_3/\text{TiO}_2$ ratios (<18) and higher $(\text{Gd}/\text{Yb})_N$ values. In this study bivariate plots of $(\text{Gd}/\text{Yb})_N$ versus $\text{CaO}/\text{Al}_2\text{O}_3$ ratios (Fig. 21a) as well as $\text{Al}_2\text{O}_3/\text{TiO}_2$ ratios (Fig. 21b) indicate variable involvement of garnet either as residual phase during melting or garnet entering melt.

5.5.2. Constraints from trace elements

About 60 percent of samples show chondritic to sub-chondritic REE and other incompatible elements whilst remaining samples display slightly higher REE contents implying heterogeneous but

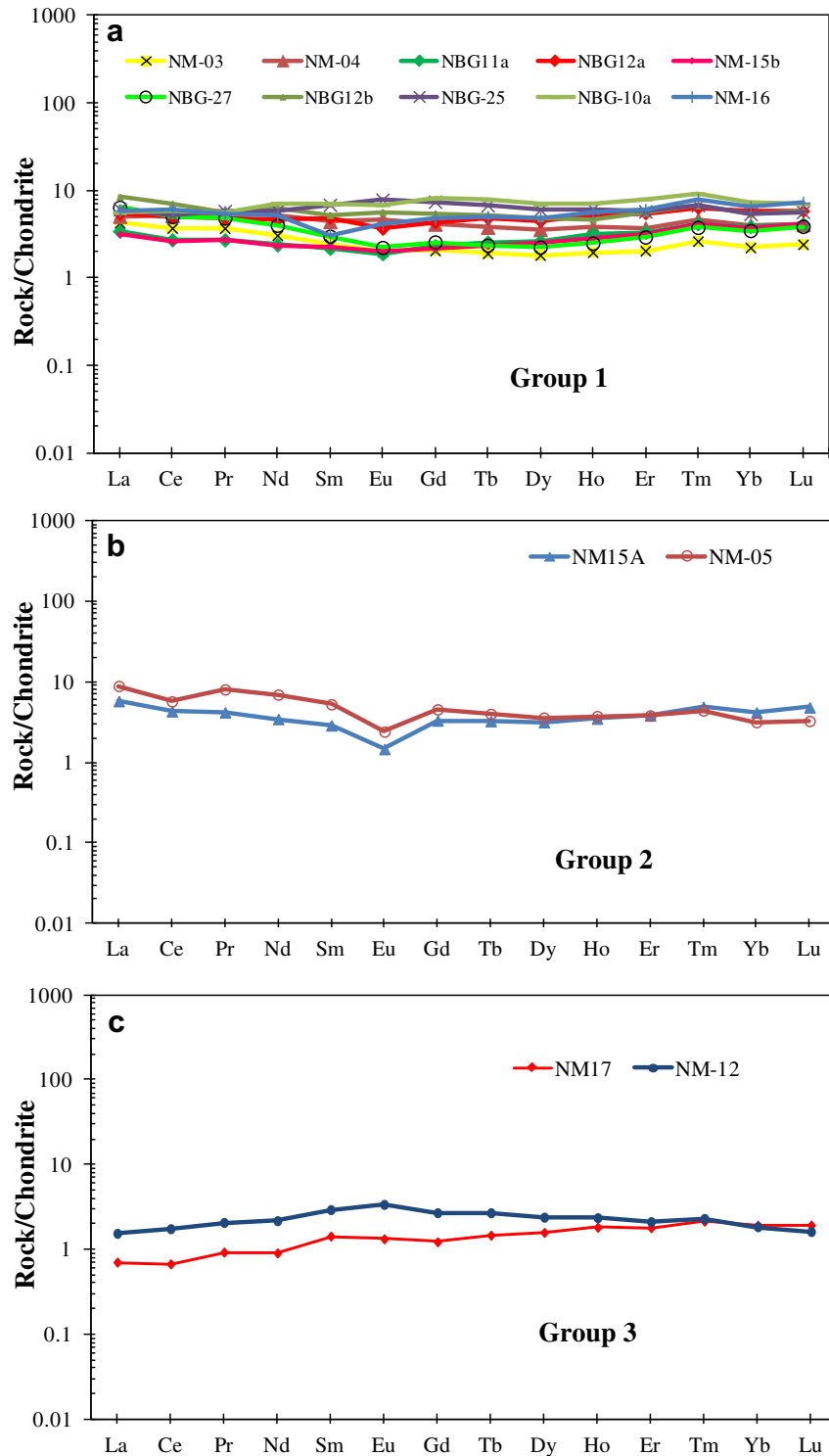


Figure 18. Primitive mantle (Sun and McDonough, 1989) normalised multi-element diagram of komatiites of Nagamangala greenstone belt.

generally depleted mantle source. The komatiitic basalts also show chondritic to sub-chondritic REE (25–53 ppm) except one sample show slightly higher total REE (88 ppm) suggesting its derivation from a source similar to primitive mantle. Zr, Hf, Y anomalies have been used to characterize nature of sources and composition of melt residues (Xie et al., 1993; Fan and Kerrich, 1997; Polat et al., 1999). Strong negative Zr and Hf anomalies in Al-depleted komatiites from Barberton greenstone belt and Superior province

reflect their derivation from deep mantle melt segregation in a plume with residual majorite garnet at depths of 400 km (Lahaye et al., 1995; Polat et al., 1999). We interpret the observed moderate to strong negative Zr and Hf anomalies with relatively flat HREE in Al-depleted and Al-undepleted komatiites as reflecting the melt generation at different depths (around 350–250 km) in mantle. On the other hand the absence of Zr anomalies in komatiite basalts together with Al-undepleted character can be attributed to

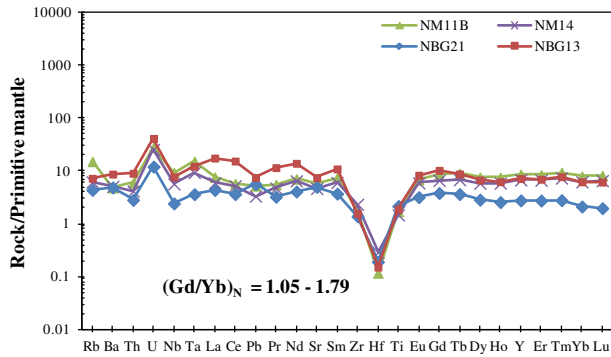


Figure 19. Primitive mantle (Sun and McDonough, 1989) normalised multi-element diagram of komatiite basalt of Nagamangala greenstone belt.

shallower melting of mantle (shallower mantle around 250 km depth) for the melt generation.

Nb anomalies on the primitive mantle-normalised multi-element spider diagrams have been used to characterize different mantle sources as well as a powerful tectonic discriminate between plume and arc settings (Jochum et al., 1991; Puchtel et al., 1997). Strong negative Nb anomalies have been explained in terms of magma generation at shallower mantle in arc environments or even crustal contamination processes (Polat and Kerrich, 2000). On the contrary positive Nb anomalies have been attributed to their derivation from plume source that contain recycled slab material at greatest mantle depths (Kerrich and Xie, 2002). However, the thermo-mechanical processes of Mesoproterozoic lateral accretion and rates of down going oceanic slabs are not clearly understood, but lateral movement and rates of down going slabs including their recycling are considered to be faster during Archaean (Fyfe, 1978). Majority of the studied komatiites from Nagamangala greenstone belt show either zero or slight positive Nb anomalies on primitive mantle-normalised multi-element spider diagrams implying magma generation from a plume source possibly involving recycled slab component. Lack of Nb anomalies and/or positive Nb anomalies in komatiites in Sargur Group greenstone sequences in western Dharwar craton have been interpreted by their derivation from mantle plume containing recycling slab component (Jayananda et al., 2008) which could also be substantiated by earlier episodes of crustal growth in arc settings (Naqvi et al., 2009). On the other hand studied komatiite basalts and one sample of komatiite (NBG 12) showing negative Nb anomalies together with absence of Zr anomalies on spider diagram could be attributed to their derivation from shallower mantle with garnet melting or elimination of garnet before melt acquires ultramafic composition (Arndt, 2003). Alternatively observed negative Nb anomalies in few samples can be also explained by contamination with ancient continental crust. However, the low-SiO₂ contents together with high Ni, Cr and low LREE are not in agreement with large-scale crustal contamination. Those studied Al-depleted komatiite samples with strong negative Hf anomalies and corresponding higher (Gd/Yb)_N values (>1.0)

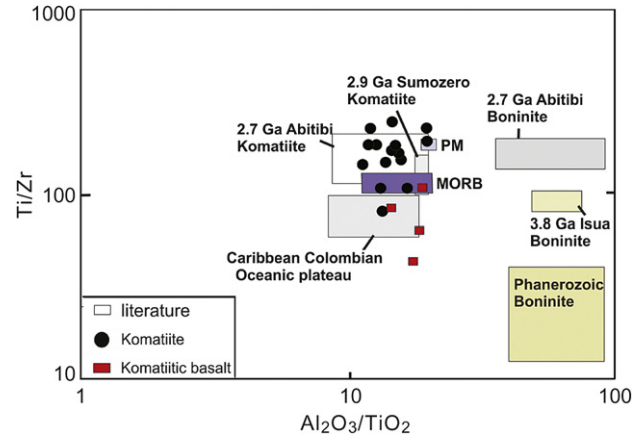


Figure 20. Ti/Zr versus Al₂O₃/TiO₂ diagram for komatiites and komatiite basalts of Nagamangala belt.

coupled with lower HREE levels compared primitive mantle possibly derived melt segregation from deep mantle with influence of residual garnet (majorite?) in the source. On the contrary, samples of komatiites and komatiite basalts with low (Gd/Yb)_N values (<1.0) coupled with absence of Hf anomalies and higher Zr, Y, HREE contents can be attributed to their melt generation in the shallower levels without involvement of garnet residue. Consequently the observed range of (Gd/Yb)_N values, Hf, Zr, Y anomalies and HREE levels indicate magma generation at different depths (approximately 350–250 km) in the mantle with or without involvement of residual garnet.

5.5.3. Melting processes and temperature of komatiite magmas

Hanson and Langmuir (1978) modelled partial melting of mantle melting using the equations of Roeder and Ernsie (1970) for the partitioning of magnesium and iron between olivine and melt, they calculated the abundances of MgO and FeO in the resultant melts and residual solids. The results are presented in MgO-FeO diagram which show a field of melts and of residual solids, both contoured for percentage of partial melting and temperatures. Fractional crystallization trends of olivine in melts of differing composition superposed on the melt field. The MgO-FeO diagram of Hanson and Langmuir (1978) can also give information on the liquidus temperatures of magmas. In addition olivine fractional crystallization paths may be plotted for a given melt composition. In the present study this diagram has been used to evaluate the relationship between komatiites and komatiite basalts. Our data projected on the MgO-FeO diagram (Fig. 22) show that only komatiites plot in the field of liquids probably co-existed with mantle peridotite. On the other hand the komatiite basalts plot outside the liquidus field defined, which could be related to their melts accumulation in shallow mantle or not in equilibrium with mantle peridotite. The komatiites were generated by generally high degree (20–50%) partial melting of mantle with initial liquidus

Table 2
Published geochronology of the greenstone belt of western Dharwar craton.

SL. No.	Method	Age	WDC greenstone belts	Authors
1	SHRIMP U-Pb	3298 ± 7 Ma	Holenarsipur belt	Peucat et al., 1995
2	Sm-Nd whole rock isochron	3552 ± 110 Ma	J.C. Pura, Bansandra, Kalyadi and Nuggihalli	Jayananda et al., 2008
3	Sm-Nd whole rock isochron	3384 ± 200 Ma	J.C. Pura komatiites	Jayananda et al., 2008
4	Sm-Nd whole rock isochron	3284 ± 310 Ma	Kalyadi and Nuggihalli	Jayananda et al., 2008
5	Pb-Pb whole rock isochron	3156 ± 170 Ma	Nuggihalli belt	Mondal et al., 2008
6	Sm-Nd whole rock isochron	3136 ± 200 Ma	Banasandra greenstone belt	Maya et al., 2011

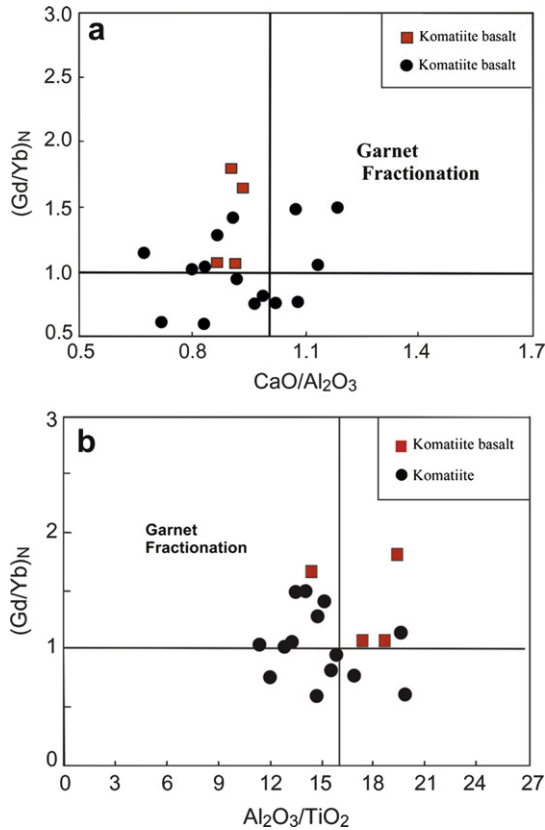


Figure 21. (a) $(\text{Gd}/\text{Yb})_N$ ratios versus $\text{CaO}/\text{Al}_2\text{O}_3$ plot for komatiites and komatiite basalt of Nagamangala greenstone belt. (b) $(\text{Gd}/\text{Yb})_N$ ratios versus $\text{Al}_2\text{O}_3/\text{TiO}_2$ plot for komatiites and komatiite basalt of Nagamangala greenstone belt.

temperatures as high as 1500 °C. In summary komatiites and komatiite basalts derived from different depths and related to different degree of melting.

5.5.4. Archaean mantle evolution and crustal growth connection

The time window of 3.4–3.2 Ga is important period in Earth history as large-scale accretion of continental crust in the form of coeval greenstone volcanism, emplacement of voluminous TTG suites and deposition of thick sedimentary sequences documented in several Archaean cratons (Condie, 1998; Kroner et al., 1996; Jayananda et al., 2008). Archaean greenstone volcanism provides much insight into our understanding of Archaean tectonics, continental growth and mantle evolution (Polat et al., 1999; Polat and Kerrich, 2000; Jayananda et al., 2008). Published geochemical and isotopic data show that continental crust has grown at the expense of mantle through partial melting processes (Rudnick, 1995). Several studies also show episodic outbursts of continental crust through mantle overturn events (Stein and Hofmann, 1994). However, the mechanisms of continental crust formation and mantle melting processes are still subjects of much discussion over years (De-Witt et al., 1987, 1992; Choukroune et al., 1994; Hamilton, 1998; Condie, 1999).

In the Dharwar craton geochronologic and geochemical data including Nd and Pb isotopes show major continental growth during 3.4–3.2 Ga in the form of greenstone volcanism, TTG accretion (Bhaskar Rao et al., 1992; Meen et al., 1992; Nutman et al., 1992; Peucat et al., 1993, 1995; Jayananda et al., 2008; Chardon et al., 2011). Recent elemental and Nd isotope data on 3.35 Ga komatiites from WDC show existence of depleted mantle reservoirs which in turn would imply an earlier episode of continental growth in the form of earlier plume related greenstone volcanism probably during 3.6–3.5 Ga (Jayananda et al., 2008). The lithospheric mantle

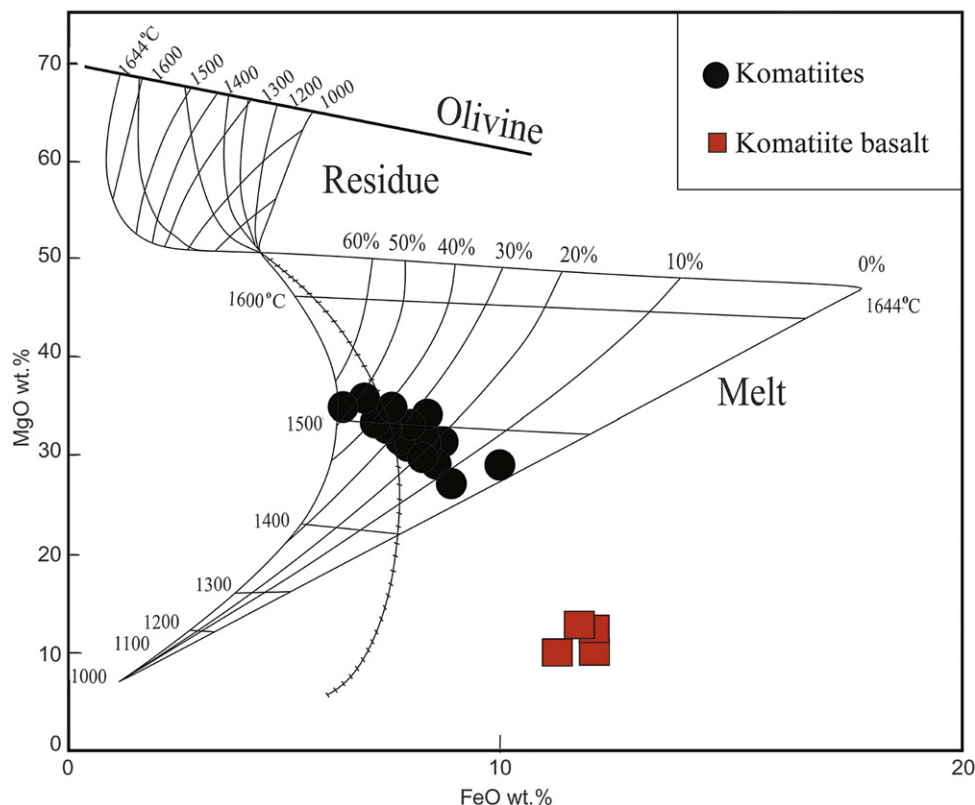


Figure 22. MgO versus FeO (wt.%) – fields of partial melts and residue (after Hanson and Langmuir, 1978) of komatiites from Nagamangala greenstone belt.

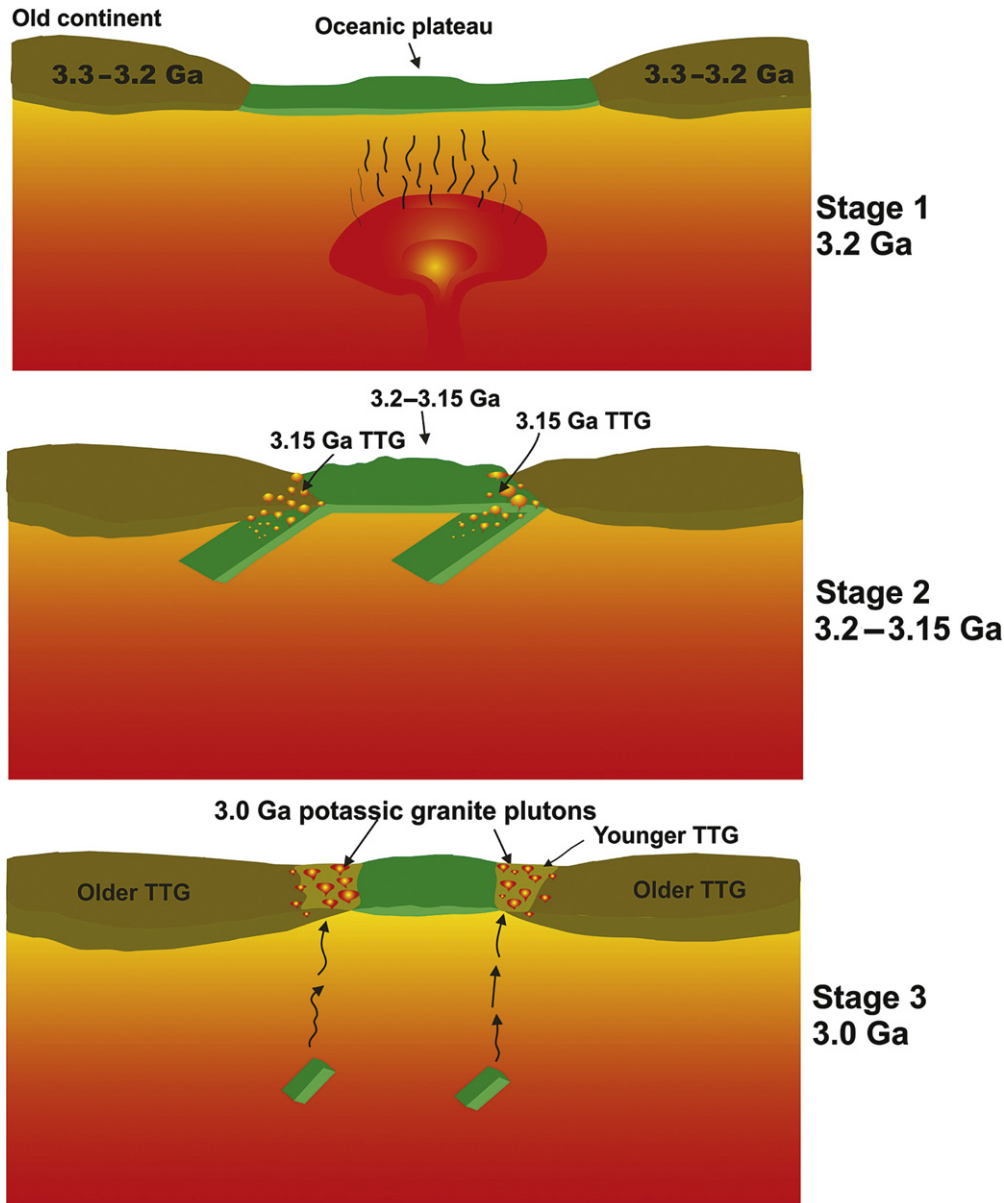


Figure 23. Cartoon showing plume-arc model for the formation of komatiites in the Nagamangala greenstone belt and adjoining sub-contemporaneous TTG in WDC.

also depleted as a consequence of extraction of magmatic protoliths of oldest crustal remnants (Gorur-type gneisses) and provenance of 3.58 Ga sediments. In the present study, majority of the komatiites and komatiite basalts show chondritic or sub-chondritic incompatible elements particularly LREE indicating their derivation from depleted mantle reservoirs during ca. 3.2–3.15 Ga. Existence of such depleted mantle reservoirs can be attributed to an earlier episode of deep mantle melting in the form of an earlier cycle of greenstone volcanism. Published ages together with Nd isotope data in the WDC are in agreement with the above argument as widespread eruption of bimodal greenstone volcanics 3.35–3.38 Ga and TTG accretion documented (Meen et al., 1992; Nutman et al., 1992; Jayananda et al., 2008). Consequently elemental data of the Nagamangala komatiites and komatiite basalts indicate depleted mantle source. The existence of depleted mantle sources during 3.2–3.15 Ga can be attributed to an earlier episode of greenstone volcanism contributing to continental growth.

5.5.5. Tectonic context of greenstone volcanism

The tectonic context of komatiite magma generation and eruption is still a subject of discussions and debate. Globally studies conducted during the past three decades lead to an intellectual framework evolving into three groups of models involving plume, arc or combined plume-arc settings. Majority of the workers propose either plume setting (Ohtani et al., 1989; Arndt et al., 1997; Kerrich and Xie, 2002; Arndt, 2003) or oceanic plateau originated from deep seated mantle plume (Kerr et al., 1996; Polat and Kerrich, 2000) whilst few propose combined plume-arc setting (e.g. Puchtel et al., 1999; Jayananda et al., 2008) or arc environment (Parman et al., 1997, 2001; Grove et al., 1999). In the WDC both uniformitarian models involving lateral accretion of arcs (Naqvi et al., 2009) and non-uniformitarian models involving vertical accretion of crust in hot spot environments are associated with rising mantle plume (Choukroune et al., 1994). More recently Jayananda et al. (2008) have proposed a combined plume-arc model to explain 3.35 Ga komatiite dominated greenstone volcanism and accretion of sub-contemporaneous TTG in the WDC.

Any tectonic model that proposes for komatiite volcanism in the Nagamangala greenstone belt must also account sub-contemporaneous accretion of surrounding TTG basement. Further, published isotopic age data of komatiites from neighbouring Sargur Group greenstone belts and their surrounding TTG basement indicate sub-contemporaneous nature. In the following section we discuss various models to explain the tectonic context of komatiite magma generation and eruption within the regional geological framework of WDC.

5.5.5.1. Subduction related arc settings. Lateral accretion of crust in arc environments is considered to be an important process for the origin of Archaean cratons (Martin and Moyen, 2002; Smithies et al., 2003). This model particularly explains the formation of TTG crust through secular changes in the angle of subduction and depth of melting in response to decreasing geothermal gradients through time (Martin and Moyen, 2002). Recently Parman et al. (1997, 2001) proposed subduction zone model to explain 3.45 Ga Barberton komatiites. However, this model has been debated (Arndt, 2003; Chavagnac, 2004; Jayananda et al., 2008) as it cannot account the chemical characteristics of komatiites particularly Al-depletion, positive Nb anomalies, high MgO, Nb/U, Nb/Th, Nb/La and Th/U ratios and high eruption temperatures of Archaean komatiites close to 1600 °C. Mafic magmas generated in subduction related arc settings are characterized by strong negative Nb anomalies in the primitive mantle-normalised multi-element diagrams. Consequently arc setting can be ruled out for komatiite and komatiite basalt volcanism in the Nagamangala belt.

5.5.5.2. Plume model. Several geochemical and isotope studies conducted on Archaean komatiites provide new constraints on the magma generation and eruption. The high magnesium contents, low incompatible elements together with highest eruption temperatures (1600–1700 °C) lead to the conclusion that these ultramafic magmas are generated by high degree of melting of mantle at great depths, in the ascending hottest portions of mantle plume (Campbell et al., 1989; Arndt, 2003; Chavagnac, 2004; Jayananda et al., 2008).

The studied komatiite and komatiite basalt samples show high content of MgO, low incompatible elements (chondritic to sub-chondritic LREE), variable Al-depletion, and absence of Nb anomalies together with strong negative Hf anomalies consistent with their generation in hot spot environments in deeper mantle (350–250 km depth) associated with rising mantle plume. The observed geochemical characteristics together with high eruption temperatures (~1500 °C) and great depth of magma generation favour a mantle plume setting for komatiite and komatiite basalts of Nagamangala greenstone belt. However, the plume model alone does not account the formation of sub-contemporaneous TTG basement. Alternatively a combined plume-arc model can be considered to explain lithological patterns and time framework greenstone volcanism, TTG accretion and emplacement of potassic granites.

5.5.5.3. Combined plume-arc model. Published ages of Sargur Group greenstone volcanics and their surrounding TTG suites indicate sub-contemporaneous nature of their formation. The close lithological association and sub-contemporaneous nature but contrasting elemental characteristics of komatiite-rich greenstone sequences and surrounding TTG require distinct geodynamic settings: (a) the 3.3–3.1 Ga surrounding TTG appears to have formed by hydrous melting of down going oceanic slab within plagioclase stability field (Martin, 1986); (b) plume derived 3.2–3.15 komatiites and komatiite basalts in greenstone sequences corresponds to remnants of oceanic plateaus; and (c) elemental and

isotopic data of 3.0 Ga potassic granites intrusive into Nagamangala belt represent reworked TTG at lower crustal levels (Jayananda et al., in prep.).

The elemental data of the studied komatiites and komatiitic basalts particularly depleted LREE do not show any involvement of older crust in their genesis or significant crustal contamination. Consequently it appears that plume has initiated beneath the oceanic crust far from sizable ancient continental land mass (Fig. 23). The komatiites from Sargur Group greenstone sequences display pillow structures point to their eruption in oceanic environments. Isotopic age data indicate the time difference between plume derived ultramafic volcanic rocks and surrounding TTG is about 30–50 Ma (Peucat et al., 1993, 1995; Bidyananda et al., 2003; Jayananda et al., 2008; Mondal et al., 2008; Maya et al., 2011). Abbott et al. (1994) have convincingly shown that a plume has the thermal potential to produce a thick komatiitic to basaltic oceanic plateau with an average thickness of ~35 km. Oceanic plateaus of such great thickness are typically underlain by more refractory lithospheric mantle roots buoyant enough to resist subduction (Cloos, 1993; Abbot and Mooney, 1995). In this kind of situation rapid subduction of intervening hot oceanic crust and melting within plagioclase stability field generate parental magmas of TTG (see Fig. 23). Magmas generated in subduction zone and their eventual crystallization at deep levels results in formation of TTG suites. Closure of arcs and break off of down going slabs probably initiated a hot spot which caused reworking of lower crustal TTG leading to formation of high-potassic granites which emplaced close to 3.0 Ga (Jayananda et al., in prep.).

6. Conclusions

The conclusions of this work can be summarized as follows:

- (1) Widespread komatiite and komatiite basalt volcanism in Nagamangala greenstone belt possibly during ca. 3.2–3.15 Ga.
- (2) Komatiites and komatiite basalts derived by melting of mantle at different depths (350–250 km) with or without influence of residual garnet in source and komatiite magmas were co-existed in equilibrium with mantle peridotite with solidus temperatures as high as 1500 °C.
- (3) Trace element data particularly incompatible element content suggest that the komatiites are derived from depleted mantle.
- (4) The existence of depleted mantle at ca. 3.2–3.15 Ga implies that upper mantle has already lost a melt component in an earlier episode of greenstone volcanism.
- (5) The komatiite volcanism and surrounding sub-contemporaneous TTG accretion can be explained by combined plume-arc model.

Acknowledgements

This work is funded by DST, Government of India in the form of Transect Project (ESS/16/334/2007/dated 14-10-2008) and DU R & D Programme. R.V. Gireesh, N.V. Jagadeesh, Kowete - Ü Sekhama, Kowe Ü-Kapfo and Alibur Rehman are thanked for support. Dr. M. Mohanty and Dr. Ch. Sivaji thanked for support. Dr. V. Balaram and Dr. N. Satyanarayanan from National Geophysical Research Institute (NGRI), Hyderabad gratefully acknowledged for analytical support. Constructive reviews by anonymous reviewer and editorial comments of Prof. M. Santosh have greatly helped to improve the quality of presentation.

Appendix A. Analytical procedures

The least altered samples were selected for geochemical studies. Samples were crushed at Department of Geology, Centre for

Advanced Studies, University of Delhi using jaw crusher to get powder of 60–80 mesh sizes and ultimately powdered to 200 mesh size powder using agate mill. 27 samples were selected for major, trace and REE analysis. Pressed pellets were made for major elements determination by X-ray fluorescence spectrometry (XRF, Philips 1400) at the University of Delhi. It is prepared by mixing half a spoon of 200 mesh size with binder (polyvinyl alcohol) in an agate mortar thoroughly and then pressed under hydraulic pressure of about 15,000 kg/cm². Trace elements including REE were analyzed by using ICP-MS (Perkin Elmer ELAN DRC II) at National Geophysical Research institute, Hyderabad (NGRI) using the following dissolution method: accurately weighed 50 mg of the rock sample powder was taken in a 100 mL Teflon beaker and 10 mL of acid mixture consisting of 7:3:1 proportion of HF, HNO₃ and HClO₄ was added and kept overnight with lids on the beakers. Next day the beakers were transferred on to a hot plate at 250 °C, heated for 30 min and then the lids were removed and the beakers reheated until dryness. Another 10 mL of the acid mixture is added in the same proportions to the sample in the beakers and dried completely. Then 5 mL of 1 ppm rhodium (Rh) is added with 20 mL of 1:1 HNO₃ and the beakers were kept on the hot plate under a warm condition for 15 min. The solutions were cooled and transferred to a 250 mL volumetric flask and the required volume is made. 60 mL of the solution is taken in a poly propylene bottle for analysis using ICP-MS. Chondrite normalised ratios were calculated using Leedy Chondrite values and primitive mantle-normalised ratios were calculated from the values of Sun and McDonough (1989).

References

- Abbot, D., Mooney, W., 1995. The structural and geochemical evolution of the continental crust: support for the oceanic plateau model of continental growth. *Supplementary Reviews of Geophysics* 33, 231–242.
- Abbott, D.H., Burgess, L., Longhi, J., Smith, W.H.F., 1994. An empirical thermal history of the earth's upper mantle. *Journal of Geophysical Research* 99, 13835–13850.
- Anand, R., Balakrishnan, S., 2010. Pb, Sr and Nd isotope systematics of metavolcanic rocks of the Hutt greenstone belt, Eastern Dharwar craton: constraints on age, duration of volcanism and evolution of mantle sources during Late Archean. *Journal of Asian Earth Sciences* 39, 1–11.
- Anil Kumar, Bhaskar Rao, Y.J., Sivaraman, T.V., Gopalan, K., 1996. Sm–Nd ages of Archean metavolcanics of the Dharwar craton, south India. *Precambrian Research* 80, 205–216.
- Arndt, N.T., 1994. Archean komatiites. In: *Condie, K.C. (Ed.), Archean Crustal Evolution*. Elsevier, Amsterdam, pp. 11–44.
- Arndt, N.T., 2003. Komatiites, kimberlites and boninites. *Journal of Geophysical Research* 108 (B6), 2293.
- Arndt, N., 2008. Komatiite, first ed. Cambridge University Press, New York.
- Arndt, N.T., Nisbet, E.G., 1982. Komatiites. *George Allen and Unwin Publ.*, UK, 526 p.
- Arndt, N.T., Teixeira, N.A., White, W.M., 1989. Bizarre geochemistry of komatiites from the Crixas greenstone belt, Brazil. *Contributions to Mineralogy and Petrology* 101, 187–197.
- Arndt, N.T., Kerr, A.C., Tarney, J., 1997. Dynamic melting in plume heads: the formation of Gorgana komatiites and basalts. *Earth and Planetary Science Letters* 146, 289–301.
- Balakrishnan, S., Hanson, G.N., Rajamani, V., 1990. Pb and Nd isotope constrains on the origin of high Mg and tholeiitic amphibolites, Kolar Schist Belt, South India. *Contributions to Mineralogy and Petrology* 107, 279–292.
- Balakrishnan, S., Rajamani, V., Hanson, G.N., 1999. U–Pb ages for zircon and titanite from the Ramagiri area, Southern India: evidence for accretionary origin of the eastern Dharwar craton during the late Archean. *Journal of Geology* 107, 69–86.
- Bau, M., 1981. Rare earth mobility during hydrothermal and metamorphic fluid-rock interaction and the significance of the oxidation state of europium. *Chemical Geology* 93, 219–230.
- Berry, A.J., Danyashevsky, L.V., O'Neill, Hugg St. C., Newville, M., Sutton, S.R., 2008. Oxidation state of iron in komatiite melt inclusions indicates hot Archean mantle. *Nature* 455, 960–963.
- Bhaskar Rao, Y.J., Sivaraman, T.V., Pantulu, C.V.C., Gopalan, K., Naqvi, S.M., 1992. Ages of late Archean metavolcanics and granites, Dharwar craton: evidence for early Proterozoic thermo-tectonic events. *Precambrian Research* 38, 246–270.
- Bidyandana, Deomurari, M.P., Goswami, J.N., 2003. ²⁰⁷Pb–²⁰⁶Pb ages of zircons from the Nuggihalli schist belt, Dharwar craton, southern India. *Current Science* 85 (10), 1482–1485.
- Braun, J.J., Pagel, M., Herbillon, A., Rosin, C., 1993. Mobilization and redistribution of REEs and thorium in a syenitic lateritic profile: A mass balance study. *Geochimica et Cosmochimica Acta* 57, 4419–4434.
- Campbell, I.H., Griffiths, R.W., Hill, R.L., 1989. Melting in an Archean mantle plume: head its basalt, tail its komatiites. *Nature* 339, 697–699.
- Chadwick, B., Ramakrishnan, M., Viswanatha, M.N., 1981. Structural and metamorphic relations between Sargur and Dharwar supracrustal rocks and peninsular gneiss in Central Karnataka. *Journal of the Geological Society of India* 22, 557–569.
- Chadwick, B., Vasudev, V.N., Hedge, G.V., 2000. The Dharwar craton, southern India, interpreted as the result of Late Archean oblique convergence. *Precambrian Research* 99, 91–101.
- Charan, S.N., Naqvi, S.M., Ramesh, S.L., 1988. Geology and geochemistry of spinifex-textured peridotitic komatiite from Mayasandra Schist Belt. *Journal of the Geological Society of India* 32, 343–350.
- Chardon, D., 1997. Less deformations continentals archeennes, exemples at modelisation thermomechanique. *Geosciences, Rennes*, unpub. thesis
- Chardon, D., Jayananda, M., Chetty, T.R.K., Peucat, J.-J., 2008. Precambrian continental strain and shear zone patterns: the South Indian case. *Journal of Geophysical Research* 113, B08402. <http://dx.doi.org/10.1029/2007JB005299>.
- Chardon, Dominique, 2011. Lateral constructional flow of hot orogenic crust: insights from the Neoproterozoic of south India, geological and geophysical implications for orogenic plateaux. *Geochemistry Geophysics Geosystems* 12 (2).
- Chardon, D., Peucat, J.-J., Jayananda, M., Choukroune, P., Fanning, C.M., 2002. Archean granite-greenstone tectonics at Kolar (South India): interplay of diapirism and bulk inhomogeneous contraction during magmatic juvenile accretion. *Tectonics* 21, 10–16. <http://dx.doi.org/10.1029/2001TC901032>.
- Chardon, D., Jayananda, M., Peucat, J.J., 2011. Lateral constrictional flow of hot orogenic crust: insights from the Neoproterozoic of south India, geological and geophysical implications for orogenic plateaux. *Geochemistry Geophysics Geosystems* 12 (2), Q02005. <http://dx.doi.org/10.1029/2010GC003398>.
- Chavagnac, V., 2004. A geochemical and Nd isotopic study of Barberton komatiites (South Africa): implication for the Archean mantle. *Lithos* 75, 253–281.
- Chikhaoui, M., 1981. Les roches volcaniques du proterozoique superieur de la chaine pan-Africaine dans le NW de l'Afrique (Hoggar, Anti-Atlas, Adrar des Iforas): caracterisation geochimique et mineralogique, implications geodynamiques, These d'Etat, Montpellier, 183 p.
- Choukroune, P., Bouhallier, H., Arndt, N.T., 1994. Soft lithosphere during periods of Archean crustal growth or crustal reworking. *Special publications* 95. In: Coward, M.P., Riess, A.C. (Eds.), *Early Precambrian Processes*. Geological Society, London, pp. 67–86.
- Cloos, M., 1993. Lithospheric buoyancy and collisional orogenesis: subduction of oceanic plateaus, continental margins, island arcs, Spreading ridges, and seamounts. *Geological Society of America Bulletin* 105, 715–737.
- Condie, K.C., 1998. Episodic continental growth and supercontinental: a mantle avalanche connection. *Earth and Planetary Science Letters* 163, 97–108.
- Condie, K.C., 1999. Mafic crustal xenoliths and the origin of the lower continental crust. *Lithos* 46, 95–101.
- De-Witt, M.J., Hart, R.A., Hart, R.J., 1987. The James down ophiolite complex, Barberton mountain belt: a section through 3.5 Ga oceanic crusts. *Journal of African Earth Sciences* 6, 681–730.
- De-Witt, M.J., Roering, C., Hart, R.J., Armstrong, R.A., Deronde, C.E.J., Green, R.W.E., Tredoux, M., Peberdy, E., Hart, R.A., 1992. Formation of an Archean continent. *Nature* 357, 451–454.
- Devapriyan, G.V., Anantharamu, T.R., Vidyadharan, K.T., Raghu Nandan, K.R., 1994. Spinifex textured peridotitic komatiite from Honnabetta area, Nagamangala schist belt, Karnataka. *Journal of Geological Society of India* 44, 483–493.
- Dostal, J., Mueller, W.U., 2012. Deciphering an Archean Mantle Plume: Abitibi Greenstone Belt, Canada. *Gondwana Research*. <http://dx.doi.org/10.1016/j.gr.2012.02.005>.
- Fan, J., Kerrich, R., 1997. Geochemical characteristics of Al-depleted and undepleted komatiites and HREE-enriched tholeiites, western Abitibi greenstone belt: variable HFSE/REE systematics in a heterogeneous mantle plume. *Geochimica et Cosmochimica Acta* 61, 4723–4744.
- Furnes, H., de Wit, M., Robins, B., 2012. A Review of New Interpretations of the Tectonostratigraphy, Geochemistry and Evolution of the Onverwacht Suite, Barberton Greenstone Belt, South Africa. *Gondwana Research*. <http://dx.doi.org/10.1016/j.gr.2012.05.007>.
- Fyfe, W.S., 1978. Evolution of the Earth's crust: modern plate tectonics to ancient hot-spot tectonics? *Chemical Geology* 23, 89–114.
- Grove, T.L., dewit, M.J., Dann, J., 1997. In: dewit, M.J., Ashwal, L.D. (Eds.), *Komatiites from the Komati Type Section, Barberton, South Africa*, in *Greenstone Belts*. Oxford Science, Oxford, U.K., pp. 422–437.
- Grove, T.L., Parman, S.V., Dann, J.C., 1999. Conditions of magma generation for Archean komatiites from the Barberton Mountain land, South Africa. In: Fei, Y., Bertla, C.M., Mysen, B.O. (Eds.), *Mantle Petrology: Field Observations and High Pressure Experimentation*. The Geochemical Society, Cadmus Journal Services, Lancaster, pp. 155–167.
- Gruau, G., Jahn, B.M., Glikson, A.Y., Davy, R., Hickman, A.H., Chauvel, C., 1987. Age of the Archean Talga-Talga subgroup, Pibara Block, Western Australia, and early evolution of the mantle: new Sm–Nd isotopic evidence. *Earth and Planetary Science Letters* 85, 105–116.
- Gruau, G., Toupin, S., Fourcade, S., Blais, S., 1992. Loss of (Nd, O) and chemical (REE) memory during metamorphism of komatiites: new evidence from eastern Finland. *Contributions to Mineralogy and Petrology* 112, 66–82.

- Hamilton, W.B., 1998. Archaean tectonics and magmatism. *International Geology Review* 40, 1–39.
- Hanson, G.N., Langmuir, C.H., 1978. Modelling of major elements in mantle-melt systems using trace element approaches. *Geochimica et Cosmochimica Acta* 42, 725–741.
- Herzberg, C., 1999. Phase equilibrium constraints on the formation of cratonic mantle. In: Fei, Y., Bertka, C.M., Mysen, B.O. (Eds.), *Mantle Petrology: Field Observations and High-pressure Experimentation*, vol. 6. Special Publication, Geochemical Society, pp. 241–257.
- Hoffman, A.W., 1988. Chemical differentiation of the Earth, the relationships between mantle, continental crust and oceanic crust. *Earth and Planetary Sciences Letters* 90, 297–314.
- Irvine, T.N., Baragar, W.R.A., 1971. A guide to the chemical classification of the common volcanic rocks. *Canadian Journal of Earth Sciences* 8, 523–547.
- Jahn, B.M., Gruau, G., Glikson, A.Y., 1982. Komatiites of the Onverwacht Group, South Africa. REE geochemistry, Sm/Nd age and mantle evolution. *Contributions to Mineralogy and Petrology* 80, 25–40.
- Jayananda, M., Peucat, J.J., 1995. Archaean crust formation in southern India geochronologic and isotopic constraints. In: Yeshida, Santosh, M., Rao, A.T. (Eds.), *India as a Fragment of East Gondwana*. Gondwana Research Group, Mem-2. Field Science Publishers, Osaka, Japan, Paper, pp. 15–21.
- Jayananda, M., Peucat, J.J., 1996. Geochronological framework of southern India. In: Santosh, M., Yoshida, M. (Eds.), *The Archaean and Proterozoic Terrains in Southern India within East Gondwana*. Gondwana Research Group Memoir, pp. 53–75.
- Jayananda, M., Moyen, J.F., Martin, H., Peucat, J.J., Auvray, B., Mahabaleswar, B., 2000. Late Archaean (2550–2520) juvenile magmatism in the eastern Dharwar craton, southern India: constraints from geochronology, Nd-Sr isotopes and whole rock geochemistry. *Precambrian Research* 99, 225–254.
- Jayananda, M., Chardon, D., Peucat, J.-J., Capdevila, R., 2006. 2.61 Ga potassic granites and crustal reworking in the western Dharwar craton, southern India: tectonic, geochronologic and geochemical constraints. *Precambrian Research* 150, 1–26.
- Jayananda, M., Kano, T., Peucat, J.J., Channabasappa, S., 2008. 3.35 Ga komatiite volcanism in the western Dharwar craton, southern India: constraints from Nd isotopes and whole rock geochemistry. *Precambrian Research* 162, 160–179. <http://dx.doi.org/10.1016/j.precamres.2007.07.010>.
- Jayananda, M., JahnB.-m., Gireesh, R.V., Bora, S., 2011. Geochronologic and isotopic constraints on the accretionary relationships of western and eastern blocks of the Dharwar craton across Huliya-Sira corridor: implications for late Archaean tectonics. *Abst. International Symposium on Precambrian Accretionary Orogens*. Geological Society of India, 51–53.
- Jayananda, M., Peucat, J.-J., Chardon, D., Krishna Rao, B., Fanning, C.M., 2012. Neorchaean greenstone volcanism and continental growth, Dharwar craton, southern India: constraints from SIMS U-Pb zircon geochronology and Nd isotopes. *Precambrian Research*. <http://dx.doi.org/10.1016/j.precamres.2012.05.002>.
- Jenson, L.S., 1976. A new method of classifying alkali volcanic rocks. Ontario Division Mineral, Miscellaneous Paper. 66, pp. 22.
- Jochum, K.P., Arndt, N.T., Hofmann, A.W., 1991. Nb-Th-La in komatiites and basalts: constraints on komatiites petrogenesis and mantle evolution. *Earth and Planetary Science Letters* 107, 272–289.
- Kerr, A.C., Marriner, G.F., Arndt, N.T., Tarney, J., Nivia, A., Saunders, A.D., Duncan, R., 1996. The petrogenesis of Gorgona komatiites, picrites and basalts: new field, petrographic and geochemical constraints. *Lithos* 37, 245–260.
- Kerrich, R., Xie, Q., 2002. Compositional recycling structure of an Archaean superplume: Nb-Th-U-LREE systematics of Archaean komatiites and basalts revisited. *Contributions to Mineralogy and Petrology* 142, 476–484.
- Kerrich, R., Wyman, D., Hollings, P., Polat, A., 1999. Variability of Nb/Th and Th/La in 3.0 to 2.7 Ga Superior province ocean plateau basalts: implications for the timing of continental growth and lithosphere recycling. *Earth and Planetary Science Letters* 168, 101–115.
- Krogstad, E.J., Hanson, G.N., Rajamani, V., 1991. U-Pb ages of zircon and sphene for two gneiss terranes adjacent to the Kolar Schist Belt, South India: evidence for separate crustal evolution histories. *Journal of Geology* 99, 801–816.
- Kroner, A., Geger, E., Wendt, J.L., Byerly, G.R., 1996. The oldest part of the Barberton granitoid-greenstone Terrain, South Africa: evidence for crust formation between 3.5 and 3.7 Ga. *Precambrian Research* 78, 105–124.
- Lahaye, X., Arndt, N.T., Byerly, G., Chauvel, C., Fourcade, S., Gruau, G., 1995. The influence of alteration on the trace-element and Nd isotopic compositions of Komatiites. *Chemical Geology* 126, 43–64.
- Leshner, C.M., Arndt, N.T., 1995. REE and Nd isotope geochemistry, petrogenesis and volcanic evolution of contaminated komatiites at Kambalda, Western Australia. *Lithos* 34, 127–157.
- Ludden, J.N., Gelinis, L., Trudel, P., 1982. Archaean metavolcanics from the Rouyn-Noranda district, Abitibi greenstone belt, Quebec. 2. Mobility of trace elements and petrogenetic constraints. *Canadian Journal of Earth Sciences* 19, 2276–2287.
- Mahabaleswar, B., Shadakshara Swamy, N., Jayananda, M., 1995. Geochemistry of metapelites from Archaean high terrain of southern Karnataka, South India. *Memoir, Geological Society of India* no. 34. In: Yoshida, M., Santosh, M. (Eds.), *India and Antarctica during Precambrian*, pp. 259–271.
- Manikyamba, C., Kerrich, R., Khanna, T.C., Satyanarayanan, M., Keshav Krishna, A., 2009. Enriched and depleted arc basalts, with Mg-andesites and adakites: A potential paired arc-back-arc of the 2.6 Ga Hutti greenstone terrane, India. *Geochimica et Cosmochimica Acta* 73, 1711–1736.
- Manikyamba, C., Kerrich, Robert, 2011. Geochemistry of alkaline basalts and associated high-Mg basalts from the 2.7 Ga Penakacherla Terrane, Dharwar craton, India: an Archean depleted mantle-OIB array. *Precambrian Research* 188, 104–122.
- Manikyamba, C., Kerrich, R.C., 2012. Eastern Dharwar Craton, India: continental lithosphere growth by accretion of diverse plume and arc terranes. *Geoscience Frontiers* 3, 225–240.
- Martin, H., 1986. The effects of steeper Archaean geothermal gradients on geochemistry of subduction zone magmas. *Geology* 14, 753–756.
- Martin, H., Moyen, J.F., 2002. Secular changes in tonalite-trondhjemite granodiorite composition as markers of the progressive cooling of earth. *Geology* 30 (4), 319–322.
- Maya, J.-M., Bhutani, R., Balakrishnan, S., 2011. ^{146,147}Sm–^{142,143}Nd studies of Komatiites from western Dharwar Craton, India: implications for depleted mantle evolution in Early Archean. *Goldschmidt Conference Abstract*. Mineralogical Magazine, p. 1430.
- Meen, J.K., Rogers, J.J.W., Fullagar, P.D., 1992. Lead isotopic composition in the western Dharwar craton, southern India: evidence for distinct middle Archaean terranes in a late Archaean craton. *Geochimica et Cosmochimica Acta* 56, 2455–2470.
- Mondal, S.K., Mukherjee, R., Rosing, M.T., Frei, R., Waight, J., 2008. Petrologic, geochemical and isotopic study of 3.1 Ga peridotite-chromite suite from western Dharwar craton (India): evidence for recycling of oceanic crust in the Mesoproterozoic. *EOS Transactions AGU* 89 (53). Fall Meeting Supplementary. Abstract. v. 33 C-2237.
- Moyen, J.-F., Martin, H., Jayananda, M., Auvray, B., 2003. Late Archaean granites: a typology based on the Dharwar Craton (India). *Precambrian Research* 127, 103–123.
- Moyen, J.F., 2011. The composite Archaean grey gneisses: petrological significance, and evidence for a non-unique tectonic setting for Archaean crustal growth. *Lithos* 123, 21–36.
- Mukherjee, R., Mondal, S.K., Rosing, M.T., Robert, F., 2010. Compositional variations in the Mesoproterozoic chromites of the Nuggihalli schist belt, Western Dharwar Craton (India): potential parental melts and implications for tectonic setting. *Contributions to Mineralogy and Petrology* 160, 865–885.
- Naqvi, S.M., Ram Mohan, M., Rana Prathap, J.G., Srinivasa Sarma, D., 2009. Adakite-TTG connection and fate of Mesoproterozoic basaltic crust of Holenarsipur Nucleus, Dharwar Craton, India. *Journal of Asian Earth Sciences* 35, 416–434.
- Nesbitt, R.W., Sun, S.S., 1976. Geochemistry of Archaean spinifex textured peridotites and magnesian low-magnesian tholeiites. *Earth and Planetary Science Letters* 31, 433–453.
- Nutman, A.P., Chadwick, B., Ramakrishnan, M., Viswanatha, M.N., 1992. SHRIMP U–Pb ages of detrital zircon in Sargur supracrustal rocks in western Karnataka, southern India. *Journal of Geological Society of India* 39, 367–374.
- Nutman, A.P., Chadwick, B., Krishna Rao, B., Vasudev, V.N., 1996. SHRIMP U–Pb zircon ages of acid volcanic rocks in the Chitradurga and Sandur groups and granites adjacent to Sandur schist belt. *Journal of Geological Society of India* 47, 153–161.
- Ohtani, E., Kawabe, I., Moriyama, J., Nagata, Y., 1989. Partitioning of elements between majorite garnet and melt and implications for petrogenesis of komatiites. *Contributions to Mineralogy and Petrology* 103, 263–269.
- Parman, S.W., Dann, J.C., Grove, T.L., de Wit, M.J., 1997. Emplacement conditions of komatiite magmas from the 3.49 Ga Komati Formations, Barberton greenstone belt, South Africa. *Earth and Planetary Science Letters* 150, 303–323.
- Parman, S.W., Grove, T.L., Dann, J.C., 2001. The production of Barberton komatiites in an Archaean subduction zone. *Geophysical Research Letters* 28, 2513–2516.
- Peucat, J.-J., Mahabaleswar, B., Jayananda, M., 1993. Age of younger tonalitic Magmatism and granulite metamorphism in the south Indian transition zone (Krisnagiri area): comparison with older peninsular gneisses from Hassan-Gorur area. *Journal of Metamorphic Geology* 11, 879–888.
- Peucat, J.-J., Bouhallier, H., Fanning, C.M., Jayananda, M., 1995. Age of Holenarsipur schist belt, relationships with the surrounding gneisses (Karnataka, south India). *Journal of Geology* 103, 701–710.
- Peucat, J.-J., Jayananda, M., Chardon, D., Capdevila, R., Fanning Marc, C., Paquette, Jean-Louis, 2012. The lower crust of Dharwar craton, south India: patchwork of Archean granulitic domains. *Precambrian Research*. under revision.
- Polat, A., Kerrich, R., 2000. Archaean greenstone belt magmatism and the continental growth-mantle evolution connection: constraints from Th-U-Nb-LREE systematics of the 2.7 Ga Wawa subprovince, Superior province, Canada. *Earth and Planetary Science Letters* 175, 41–54.
- Polat, A., Kerrich, R., Wyman, D.A., 1999. Geochemical diversity in oceanic komatiites and basalts from the late Archean Wawa greenstone belts, Superior Province, Canada: trace element and Nd isotope evidence for a heterogeneous mantle. *Precambrian Research* 94, 139–173.
- Puchtel, I.S., Hasee, K.M., Hofmann, A.W., Chauvel, C., Kulikov, V.S., Garbe-Schonberg, C.-D., Nemchin, A.A., 1997. Petrology and geochemistry of crustally contaminated komatiitic basalts from the Vetryny Belt, southeastern Baltic Shield: evidence for an early Proterozoic mantle plume beneath rifted Archean continental lithosphere. *Geochimica et Cosmochimica Acta* 61, 1205–1222.
- Puchtel, I.S., Hofmann, A.W., Amelin, Y.V., Garbe-Schonberg, C.D., Samsonov, A.V., Shchipansky, A.A., 1999. Combined mantle plume-island arc model for the formation of the 2.9 Ga sumo-zero-kenozoer greenstone belt, SE baltic shield: isotope and trace element constraints. *Geochimica et Cosmochimica Acta* 63, 3579–3595.

- Raase, P., Raith, M., Ackermann, D., Lal, R.K., 1986. Progressive metamorphism of mafic rocks from greenschist to granulite facies in the Dharwar craton of South India. *Journal of Geology* 94, 261–282.
- Raul Minas, K., Jost, H., 2006. Low and high-alumina komatiites of Goias, Central Brazil. *Journal of South American Earth Sciences* 20, 315–326.
- Roeder, P.L., Ernsie, R.F., 1970. Olivine liquid equilibrium. *Contributions to Mineralogy and Petrology* 29, 275–289.
- Rogers, A.J., Kolb, J., Meyer, F.M., Armstrong, R.A., 2007. Tectono-magmatic evolution of the Hutti-Maski Greenstone Belt, India: constrained using geochemical and geochronological data. *Journal of Asian Earth Sciences* 31, 55–70.
- Rollinson, H.R., Windley, B.F., Ramakrishnan, M., 1981. Contrasting high and intermediate pressures of metamorphism in the Archaean Sargur Schists of southern India. *Contributions to Mineralogy and Petrology* 76, 420–429.
- Rudnick, R.L., 1995. Making continental crust. *Nature* 378, 571–578.
- Sarma, D.S., Mc Naughton, N.J., Fletcher, I.R., Groves, D.I., Ram Mohan, M., Balaram, V., 2008. The timing of gold mineralization of Hutti gold deposit, Dharwar craton, South India. *Economic Geology* 103, 1715–1727.
- Sarma, D.S., Fletcher, I.R., Rasmussen, B., Mc Naughton, N.J., Ram Mohan, M., Groves, D.I., 2011. Archaean gold mineralization synchronous with late cratonization of the western Dharwar Craton, India: and xenotime in gold deposits. *Mineral Deposita* 46, 273–288.
- Smithies, R.H., Champion, D.C., Cassidy, K.F., 2003. Formation of Earth's early Archaean continental crust. *Precambrian Research* 127, 89–101.
- Srikantia, S.V., Rao, M.S., 1990. Unusual concentric structure in komatiite of Kibbanahalli Arm of Chitradurga supracrustal belt near Banasandra, Karnataka. *Journal of Geological Society of India* 36, 424–429.
- Srikantia, S.V., Venkataramana, P., 1989. The Archaean komatiites of Nagamangala supracrustal belt, Karnataka. *Journal of Geological Society of India* 33, 210–214.
- Stein, M., Hofmann, A.W., 1994. Mantle plumes and episodic crustal growth. *Nature* 372, 63–68.
- Sun, S.-S., Nesbitt, R.W., 1978. Petrogenesis of Archaean ultrabasic and basic volcanics: Evidence from rare earth elements. *Contributions to Mineralogy and Petrology* 65, 301–325.
- Sun, S.-S., 1984. Geochemical characteristics of Archaean ultramafic and mafic volcanic rocks: implications for mantle composition and evolution. In: Kroner, A., Goodwin, A.M., Hanson, G.N. (Eds.), *Archaean Geochemistry*. Springer-Verlag, Berlin, pp. 25–46.
- Sun, S., McDonough, W., 1989. Chemical and isotopic systematics of oceanic basalts: implications for mantle composition and processes. In: Saunders, A.D., Norry, M.J. (Eds.), *Magmatism in the Ocean Basins*. Geological Society of London, London, England, pp. 313–345.
- Swaminath, J., Ramakrishnan, M., 1981. Early Precambrian supracrustals of southern Karnataka. *Memoir Geological Survey of India* 112, p. 350.
- Swaminath, J., Ramakrishnan, M., Viswanatha, M.N., 1976. Dharwar stratigraphic model and Karnataka craton evolution. *Geological Survey of India Records* 107, 149–175.
- Taylor, S.R., Gordon, M.P., 1977. Geochemical application of spark source mass spectrometry. III. Element sensitivity, precision and accuracy. *Geochimica et Cosmochimica Acta* 41, 1375–1380.
- Tourpin, S., Gruau, G., Blais, S., Fourcade, S., 1991. Resetting of REE, and Nd and Sr isotopes during carbonitisation of a Komatiite flow from Finland. *Chemical Geology* 90, 15–29.
- Trendall, A.F., De Laeter, J.R., Nelson, D.R., Mukhopadhyay, D., 1997a. A precise U–Pb age for the base of Mulaingiri formation (Bababudan Group, Dharwar Supergroup) of the Karnataka craton. *Journal of Geological Society of India* 50, 161–170.
- Trendall, A.F., de Laeter, J.R., Nelson, D.R., Bhaskar Rao, Y.J., 1997b. Further zircon U–Pb age data for the Dagingikatte formation, Dharwar Supergroup, Karnataka craton. *Journal of Geological Society of India* 50, 25–30.
- Venkata Dasu, S.P., Ramakrishnan, M., Mahabaleswar, B., 1991. Sargur–Dharwar relationship around the komatiite-rich J.C. Pura greenstone belt in Karnataka. *Journal of Geological Society of India* 38, 577–592.
- Viljoen, M.J., Viljoen, R.P., Pearn, T.N., 1982. The nature and distribution of Archaean komatiite volcanics in South Africa. In: Arndt, N.T., Nisbet, E.G. (Eds.), *Komatiites*. Allen and Unwin, London, pp. 53–79.
- Viswanatha, M.N., Ramakrishnan, M., Narayana Kuttu, T.R., 1977. Possible spinifex texture in a serpentinite from Karnataka. *Journal of Geological Society of India* 18, 194–197.
- Wilson, A.H., Carlson, R.W., 1989. A Sm–Nd and Pb isotope study of Archaean greenstone belts in the Southern Kaapvaal Craton, South Africa. *Earth and Planetary Science Letters* 96, 89–105.
- Xie, Q., Kerrich, R., Fan, J., 1993. HFSE/REE fractionation recorded in three Komatiite-basalt sequences, Archaean Abitibi green stone belt: implication for multiple plume sources and depths. *Geochimica et Cosmochimica Acta* 57, 4111–4118.
- Xie, H., Hofmann, A., Hegner, E., Wilson, A., Wan, Y., Liu, D., 2012. Zircon SHRIMP dating confirms a Paleoproterozoic supracrustal terrain in the southeastern Kaapvaal Craton, southern Africa. *Gondwana Research* 21, 818–828.
- Zachariah, J.K., Hanson, G.N., Rajamani, V., 1995. Post crystallization disturbance in the neodymium and lead isotope systems of metabasalts from the Ramagiri Schist belt, South India. *Geochimica et Cosmochimica Acta* 59, 3189–3203.
- Zhai, M.G., Santosh, M., 2011. The early Precambrian odyssey of the North China Craton: a synoptic overview. *Gondwana Research* 20, 6–25.